

Backfolding of RecA-coated DNA confined beyond the Odijk regime

Toby St Clere Smithe

17 April 2015

Abstract

An analysis of data from microchannel-confinement experiments on RecA-coated DNA shows less backfolding than predicted by the wormlike chain (WLC) model in the transition out of the Odijk regime. This is demonstrated by comparing the experimental results with simulations of the WLC model.

Contents

1	Introduction and methodology	3
2	Results and discussion	4
2.1	Combined results	7
2.2	T4 results	15
2.3	λ results	21
2.4	Rejected configurations	26
3	Kymographs	28
3.1	130603-RecA-T4-wide-2	28
3.2	130603-RecA-T4-wide-3	29
3.3	130603-RecA-T4-wide-4	29
3.4	130603-RecA-T4-wide-5	30
3.5	130603-RecA-T4-wide-7	31
3.6	130607-RecA-T4-narrow-10	32
3.7	130607-RecA-T4-narrow-7	33
3.8	130607-RecA-T4-narrow-8	34
3.9	130607-RecA-T4-narrow-9	35
3.10	130607-RecA-T4-wide-1	36
3.11	130607-RecA-T4-wide-2	37
3.12	130607-RecA-T4-wide-3	38
3.13	130607-RecA-T4-wide-4	39
3.14	130607-RecA-T4-wide-5	40
3.15	130607-RecA-T4-wide-6	41
3.16	130905-RecA-T4-narrow-1	42
3.17	130905-RecA-T4-narrow-2	43
3.18	130905-RecA-T4-narrow-3	44
3.19	130905-RecA-T4-narrow-4	44
3.20	130905-RecA-T4-narrow-5	45
3.21	130905-RecA-T4-narrow-6	45
3.22	130905-RecA-T4-narrow-7	46
3.23	130905-RecA-T4-wide-1	47

3.24	130905-RecA-T4-wide-2	48
3.25	130905-RecA-T4-wide-3	49
3.26	130905-RecA-T4-wide-4	50
3.27	130905-RecA-T4-wide-5	51
3.28	130905-RecA-T4-wide-6	52
3.29	130905-RecA-T4-wide-7	53
3.30	130905-RecA-T4-wide-8	54
3.31	130924-RecA-lambda-narrow-1	55
3.32	130924-RecA-lambda-narrow-2	56
3.33	130924-RecA-lambda-narrow-3	57
3.34	130924-RecA-lambda-narrow-4	58
3.35	130924-RecA-lambda-narrow-5	59
3.36	130924-RecA-lambda-narrow-6	60
3.37	130924-RecA-lambda-wide-1	61
3.38	130924-RecA-lambda-wide-10	62
3.39	130924-RecA-lambda-wide-2	63
3.40	130924-RecA-lambda-wide-3	64
3.41	130924-RecA-lambda-wide-4	65
3.42	130924-RecA-lambda-wide-5	66
3.43	130924-RecA-lambda-wide-8	67
3.44	130924-RecA-lambda-wide-9	68

1 Introduction and methodology

In the experiments presented here, channels were used with a height of 140 nm – thereby constraining the filaments not to fluctuate in this dimension – and widths of 600 nm to 3000 nm. Filaments are funneled from a channel of one width to a channel of another width, in increasing or decreasing order. In this way, it is possible to study the changing conformation of the filament as the channel width changes. Both T4 and λ DNA were used, with the contour lengths of the coated T4 DNA ranging from 5 microns to 11 microns, and the λ DNA ranging from 8 microns to 18 microns; the different DNA types do not produce qualitatively different results under the analysis presented here.

Dorfman *et al* have made simulations of the worm-like chain model in the regime of interest, using channel dimensions similar to those employed experimentally. Here, these simulations are compared with the experimental results. Data describing the contour lengths L and linear extensions X were extracted from microscopy videos produced by Frykholm. The persistence length of RecA-coated dsDNA was taken to be 1.15 μm , as reported by Frykholm *et al* [1], and in agreement with other estimates [2].

Each video of a single channel width contains 400 frames, and there can be up to six videos – one for each width – for a single filament in a single experiment. To estimate the extensions, X , of the molecule represented in these frames, the frames were first passed through a median filter with a radius of 2, and then the maximum pixel intensity in each column was taken to provide an intensity profile along the channel. Next, a moving average (in time) of window size 3 frames and then (in space) of window size 10 pixels was computed using these intensity profiles. Finally, an error function ‘box’ curve was least-squares fitted to each such average. This was then averaged along the channel to compute the extension.

Where data was available for a particular molecule in the narrowest (600 nm) channel, the contour length L was estimated to be the mean extension of the molecule in that channel, since narrower channels force $\langle X \rangle / L$ to tend to 1. Where data was not available for the 600 nm channel (18 of 44 cases), the length was computed by fitting a path to the frames and taking the average. Finally, where the path-fitting failed (for instance because it produced a length estimate smaller than a mean extension estimate for some channel), the length was taken as the greatest of the mean extension estimates for the channels in that experiment; this occurred in the analysis of four experiments (130603-RecA-T4-wide-5, 130905-RecA-T4-wide-3, 130905-RecA-T4-wide-7, and 130924-RecA-lambda-wide-3).

There were two rejection criteria for the data. Firstly, if the kymographs suggested experimental error (such as a ‘tangled’ molecule or a molecule becoming folded during the transition between channels of different widths), which was then supported by inspection of the microscope images; see below for examples. Secondly, data were rejected if the standard deviations of either $\langle X \rangle / L$ or L exceeded 40% of the computed values; this occurred for a total of 7 data points across 4 experiments (including 130603-RecA-T4-wide-5, mentioned above; see below for details).

Plot of $\langle X \rangle / L$ against L / l_p were produced, in order to compare with the simulated results; simulated values were inferred from the plot by Dorfman. The amount of fluctuation of the filament is quantified by the ratio $\langle X \rangle / L$: where this value is near 1, the filament is mostly straight, and smaller values indicate progressively larger fluctuations or backfolding.

Since, in most of the cases, L was computed as $\langle X \rangle$ in the 600 nm channel, the simulated data were rescaled so that $\langle X \rangle / L = 1$ in the 600 nm channel.

2 Results and discussion

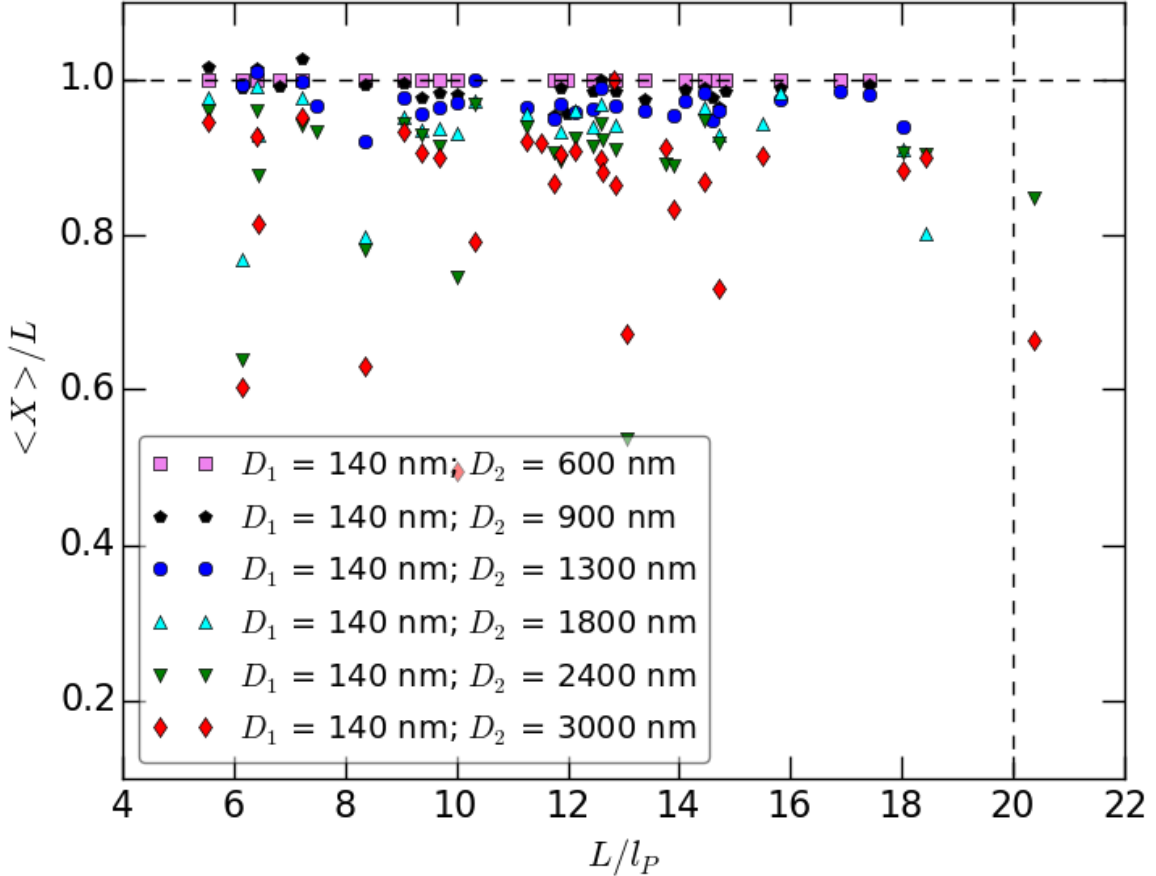


Figure 1: Experimental data; linear axes. Please note the definition of L , described above.

Having excluded the experimentally suspicious cases, of 65917 frames, 58013 were accepted according to the criteria described above (88.1%). Some examples of accepted and rejected configurations are given at the end of this report. For the different channel widths, the acceptance rates are: 91.5% (600nm), 95.8% (900nm), 86.3% (1300nm), 77.6% (1800nm), 89.8% (2400nm), and 87.8% (3000nm). More details about the rejected configurations are given below.

Some results show $\langle X \rangle > L$, but these can be explained in two ways. Firstly, in all cases, the amount by which $\langle X \rangle$ exceeds the estimate of L in each case is within one standard deviation of $\langle X \rangle$ and of L . Secondly, L is taken as the extension of the molecule as computed in the narrowest (600nm) channel – since it is here where we expect the molecule to be most extended – or, where there is no data for that channel, by fitting a path to the frames and taking the mean. However, it is not necessarily the case that in the 600nm channel, the $\langle X \rangle$ value will equal L , since there might be small fluctuations which are smaller than the microscopy resolution.

The accepted data are plotted in Figures 1 and 7. The latter has axes to match the simulated data, plotted in Figure 8, whereas the former uses linear axes to show more clearly the distribution of the points. Figures 9 to 14 show the data and simulations plotted separately for each channel width for clarity. Moreover, Figures 15 to 26 show the data and simulations, on linear axes for clarity, for the T4 and λ DNA separately, showing no significant difference.

A slight increase in the size of the fluctuations is visible given increasing channel width, but not of the same magnitude as predicted by simulations. Moreover, the negative slope for the larger

channel sizes seen in 8 is not visible in the experimental data: this slope represents the increased possibility of backfolding given a length of numerous multiples of the persistence length, and sufficient space in which to make those turns.

There are nonetheless, evident in the wider channels, four molecules whose $\langle X \rangle / L$ values fall below the simulated curve, unlike the rest of the data. These are 130607-RecA-T4-wide-4 (at $L/l_p = 8.36$), 130607-RecA-T4-narrow-9 ($L/l_p = 6.16$), 130607-RecA-T4-narrow-10 ($L/l_p = 10.00$), and 130905-RecA-T4-narrow-7 ($L/l_p = 13.05$); please refer to the corresponding kymographs at the end of this document. Moreover, 130924-RecA-lambda-wide-2 ($L/l_p = 20.37$) appears interesting, since it is a long molecule which seems naturally to adopt a much more folded configuration in the 3000nm channel than the 2400nm channel; however, it appears to display a 'knot' (see figure below) in many of the microscopy frames.

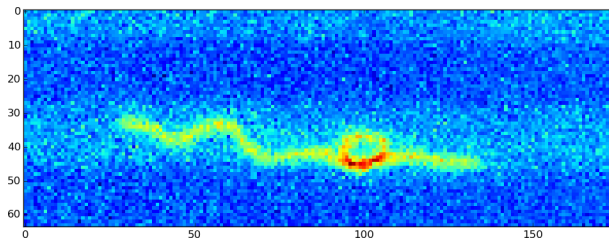


Figure 2: 130924-RecA-lambda-wide-2 at frame 131 in the 3000nm channel

130607-RecA-T4-wide-4 (which, like all experiments tagged 'wide', starts from the 3000nm channel, and moves to progressively narrower ones) folds over beginning around frame 110, unfolds substantially around frame 300, and then curls back up for the remainder of the time in that channel. A similar bimodal pattern is evident in the 2400nm channel. However, at the beginning of the 1800nm channel, one end is folded back slightly, which may be due to experimental error in the transition between channels. The molecule nonetheless unfolds at around frame 335.

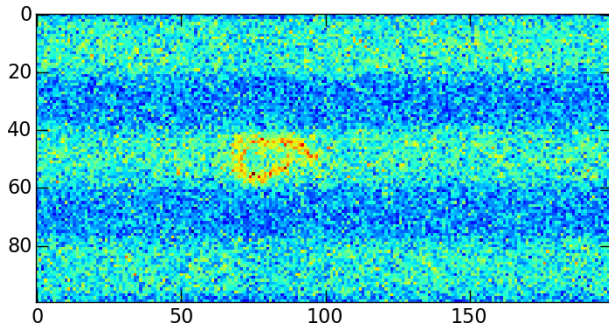


Figure 3: 130607-RecA-T4-wide-4 at frame 141 in the 3000nm channel

130607-RecA-T4-wide-4 is the one of few molecules which seem to show clearly, particularly here in the two widest channels, a coherent folded configuration that mostly does not seem to be the result of an external experimental condition. Since it shows at least two modes of configuration – folded and unfolded – the average $\langle X \rangle$ is skewed accordingly, and hence this molecule is one of few that is consistent with the simulations.

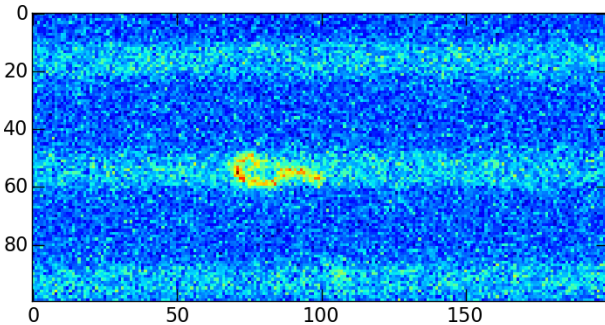


Figure 4: 130607-RecA-T4-narrow-9 at the start of the 1800nm channel sequence

130607-RecA-T4-narrow-9 is folded at the beginning of the 1800nm sequence, but it is not clear if this is an experimental error, or a natural back-fold. The molecule does seem to unfold around frame 138 of that sequence, with the folded end tumbling over the rest of the molecule until the left and right ends have switched and the molecule is extended. However, at around frame 210, the originally folded end once more folds back up against the rest of the molecule. At the beginning of the 2400nm sequence, the molecule appears quite tangled, and similar patterns are displayed for the rest of the experiment.

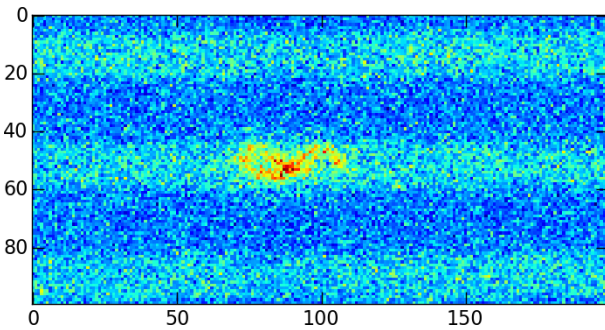


Figure 5: 130607-RecA-T4-narrow-10 at the start of the 2400nm channel sequence

130607-RecA-T4-narrow-10 is folded at the beginning of the 2400nm sequence, but unfurls beginning at around frame 175, and remains without back-folds for the rest of the sequence. At the beginning of the 3000nm sequence, it is again completely folded over, and remains at least slightly folded for the rest of the sequence. It is not clear if this is due to experimental error.

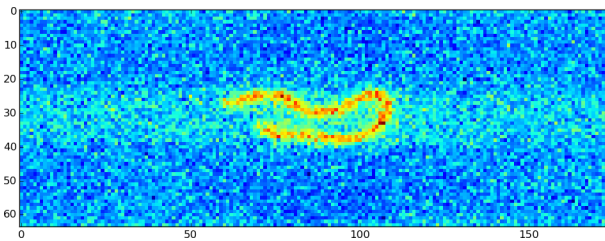


Figure 6: 130905-RecA-T4-narrow-7 at the start of the 2400nm channel sequence

Similarly, 130905-RecA-T4-narrow-7 is folded over at the beginning of the 2400nm sequence (the smallest channel for which we have data for this molecule), but it never seems to unfurl completely for the rest of the experiment.

In general, since the experimental results do not match the simulations, it is possible that the wormlike chain model, on which the simulations are based, does not apply to the RecA-

coated filaments treated here. The filaments upon which the experimental data are based are partial coated segments of a longer uncoated chain. If the WLC model is inappropriate, there are therefore two possibilities, which may both apply: (1) the coating itself affects the physics of the filament; (2) the extra uncoated bulk at either end of the filament makes fluctuations more difficult. This latter case seems possible, at least: in order for the coated filament to produce a backfold, the bulk at one end would either have to accumulate near the rest of the filament, or cross it. However, the λ DNA has less uncoated bulk at the ends of the filament (**can this be quantified?**), so it is not clear to what extent this hypothesis can explain the results.

One question to answer is, “what do the simulated distributions look like that produce the averages shown?” Knowing the answer to this would aid in verifying the distributions analysed here.

2.1 Combined results

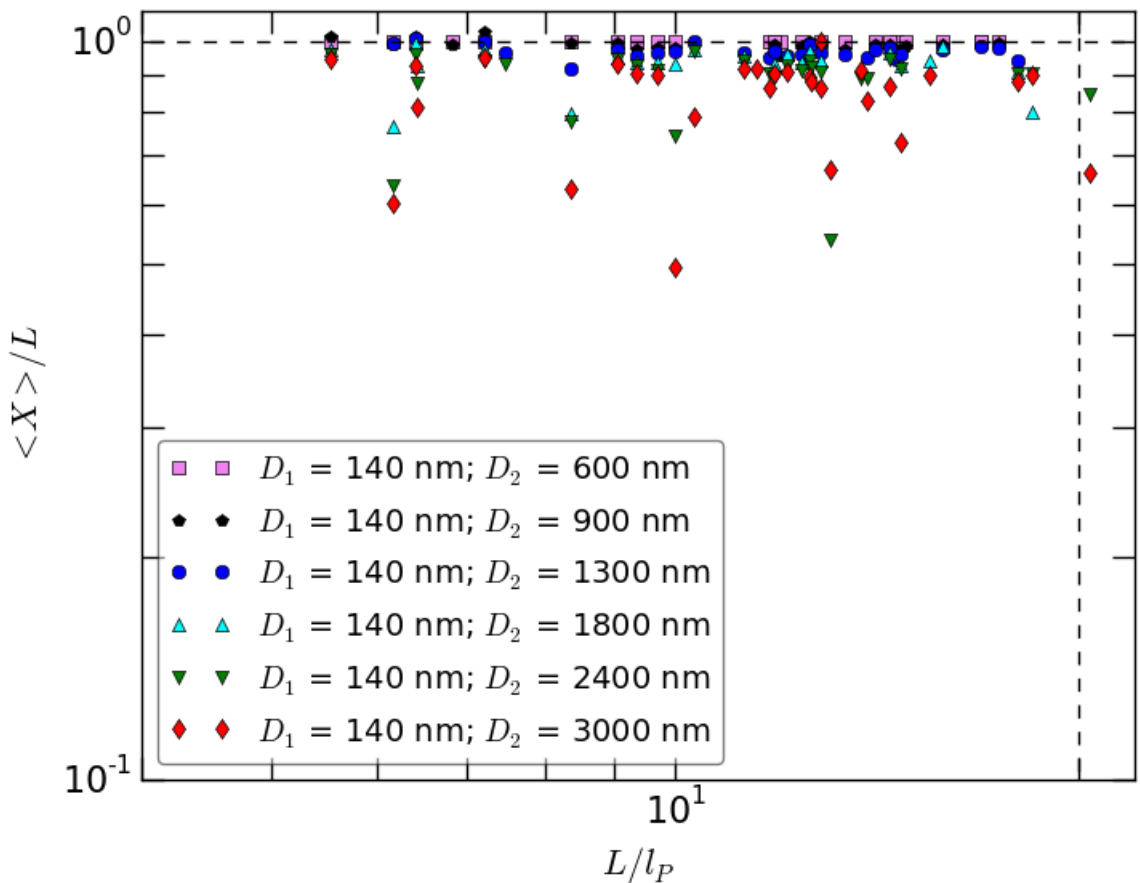


Figure 7: Experimental data; log axes. The dashed vertical line is the dashed line in 8.

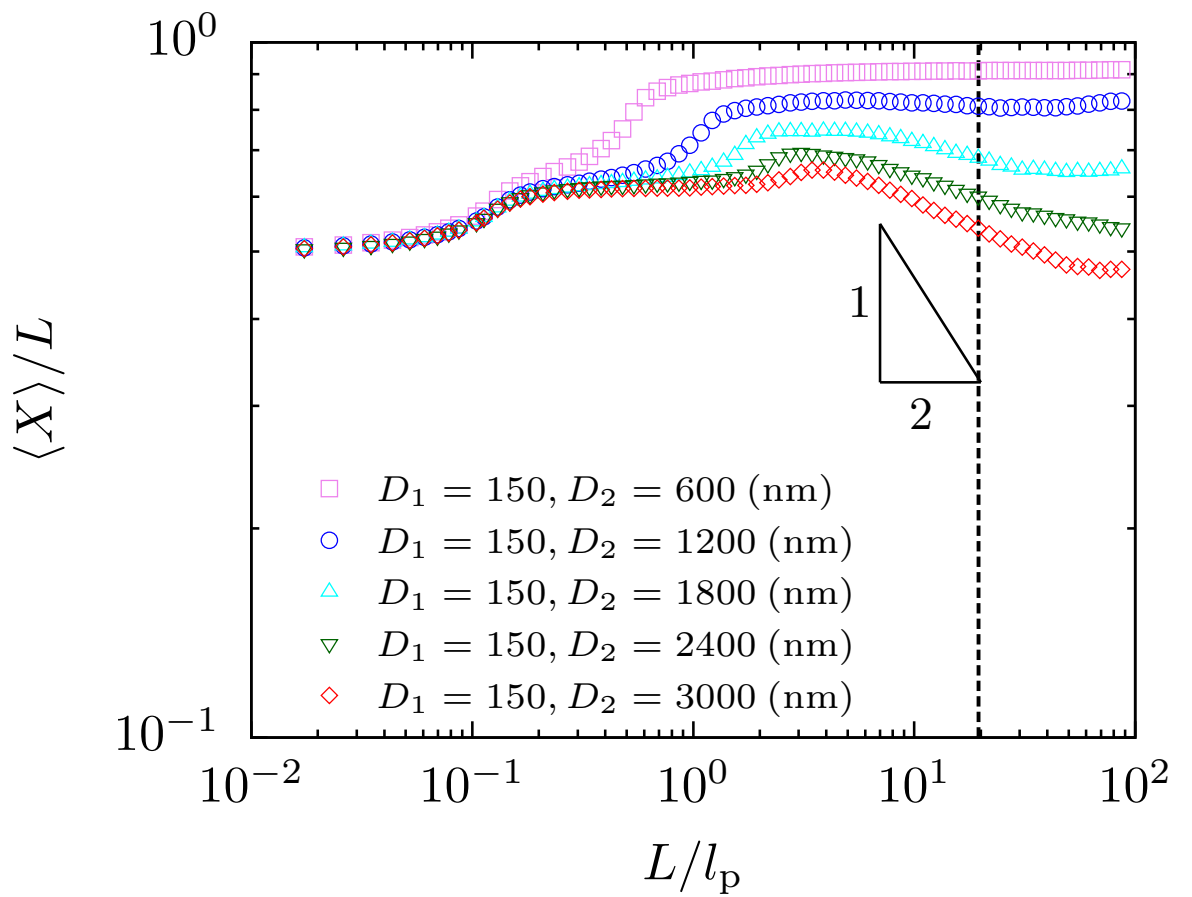


Figure 8: Simulated data, from Dorfman. Please note that the experimental data is rescaled so that the pink line equals 1.

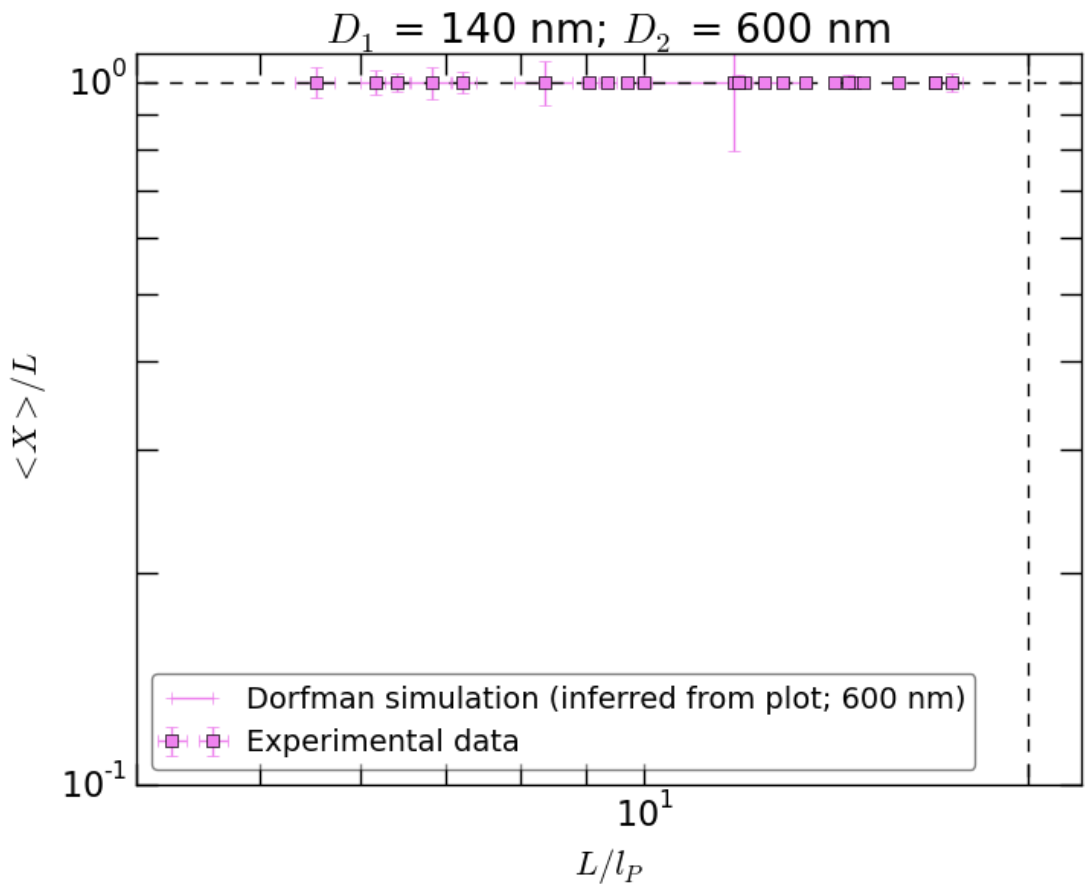


Figure 9: 600nm channel; log axes. Points represent experimental data, whilst the line represents the simulated data for the 600nm channel. The dashed vertical line is the dashed line in 8. Error bars represent one standard deviation of the quantities along each axis.

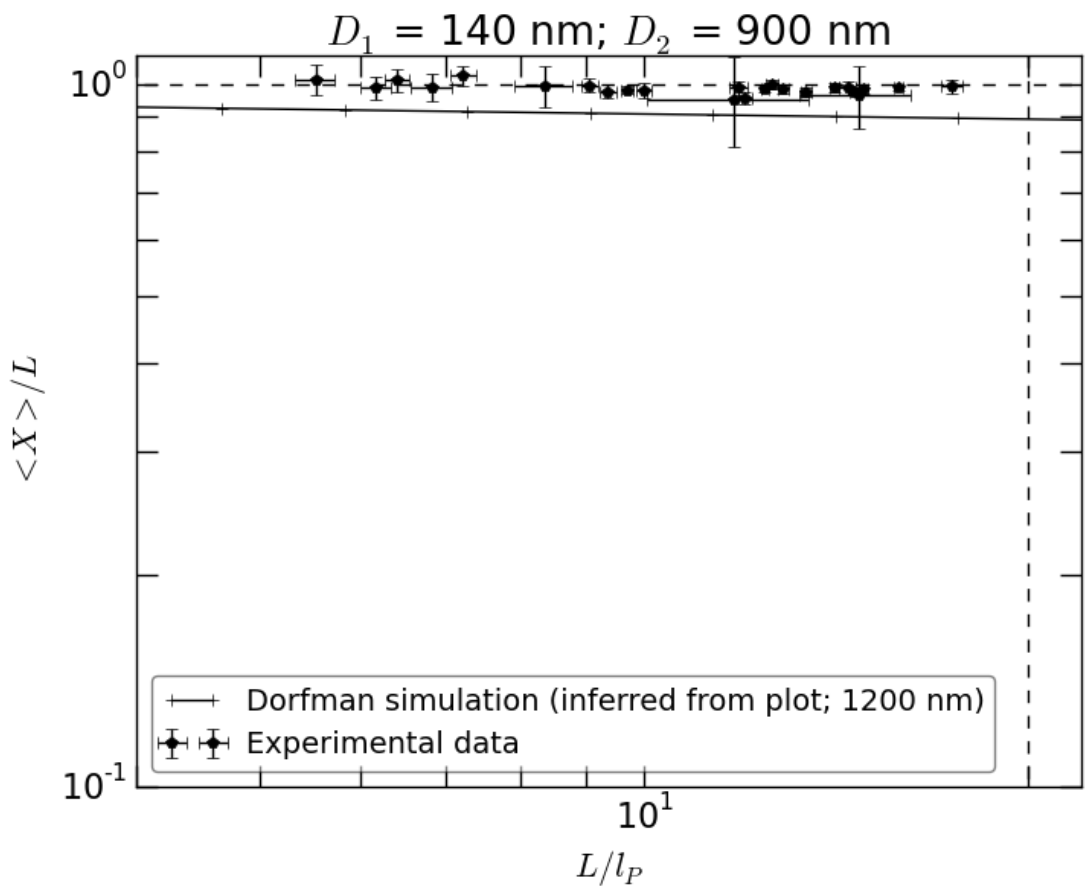


Figure 10: 900nm channel; log axes. Points represent experimental data, whilst the line represents the simulated data for the 1200nm channel. The dashed vertical line is the dashed line in 8. Error bars represent one standard deviation of the quantities along each axis.

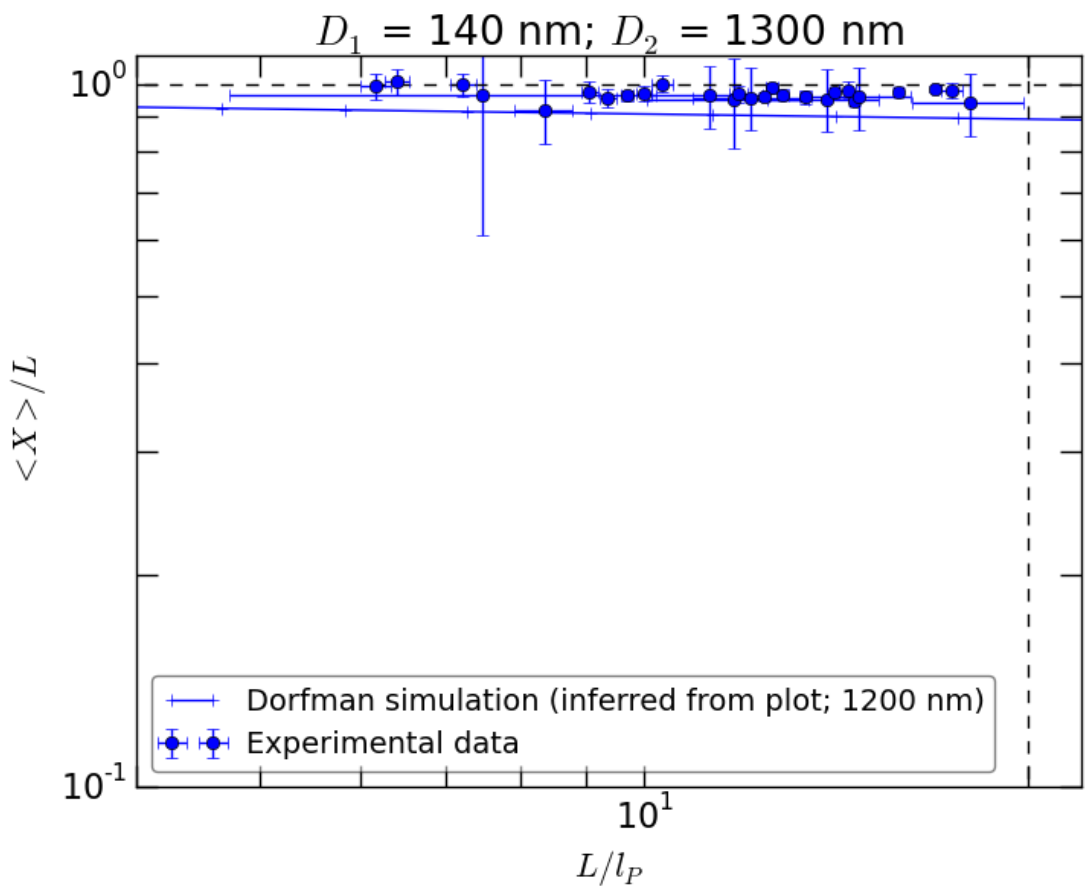


Figure 11: 1300nm channel; log axes. Points represent experimental data, whilst the line represents the simulated data for the 1200nm channel. The dashed vertical line is the dashed line in 8. Error bars represent one standard deviation of the quantities along each axis.

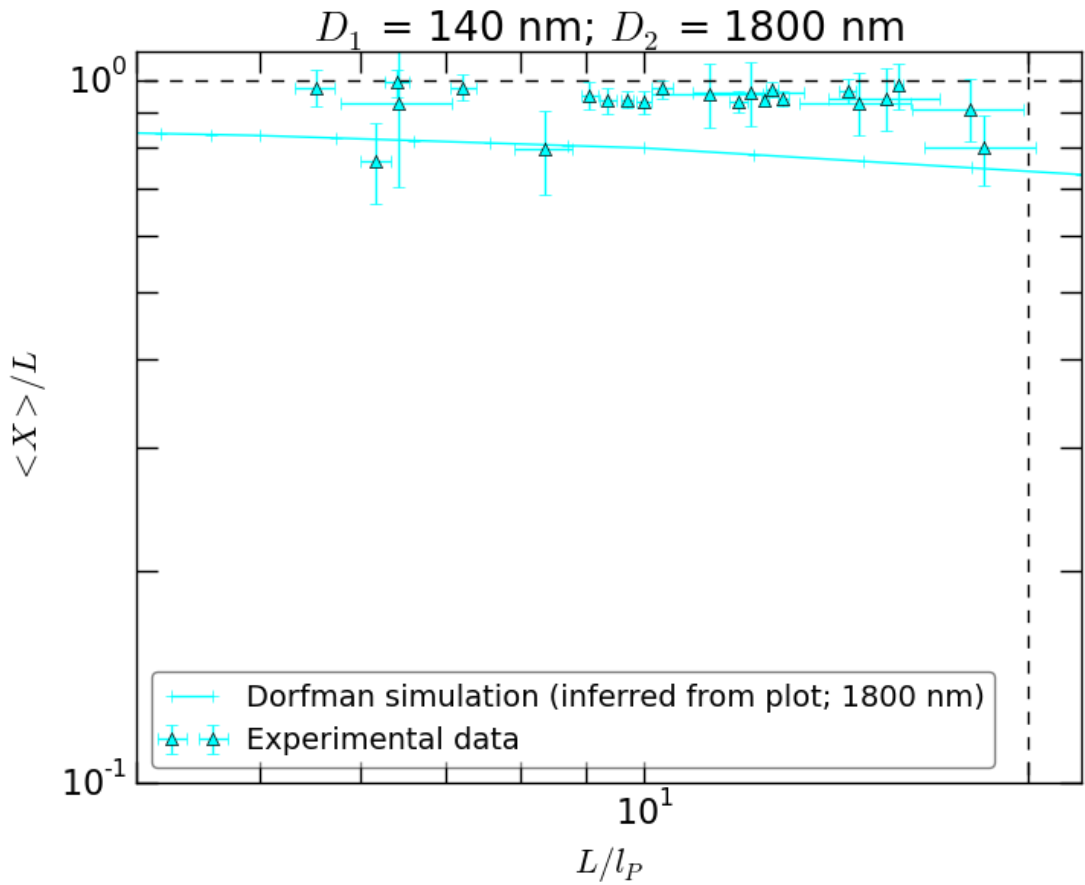


Figure 12: 1800nm channel; log axes. Points represent experimental data, whilst the line represents the simulated data for the 1800nm channel. The dashed vertical line is the dashed line in 8. Error bars represent one standard deviation of the quantities along each axis. The two lower values are 130607-RecA-T4-wide-4 (at $L/l_P = 8.36$), 130607-RecA-T4-narrow-9 ($L/l_P = 6.16$); these were discussed above.

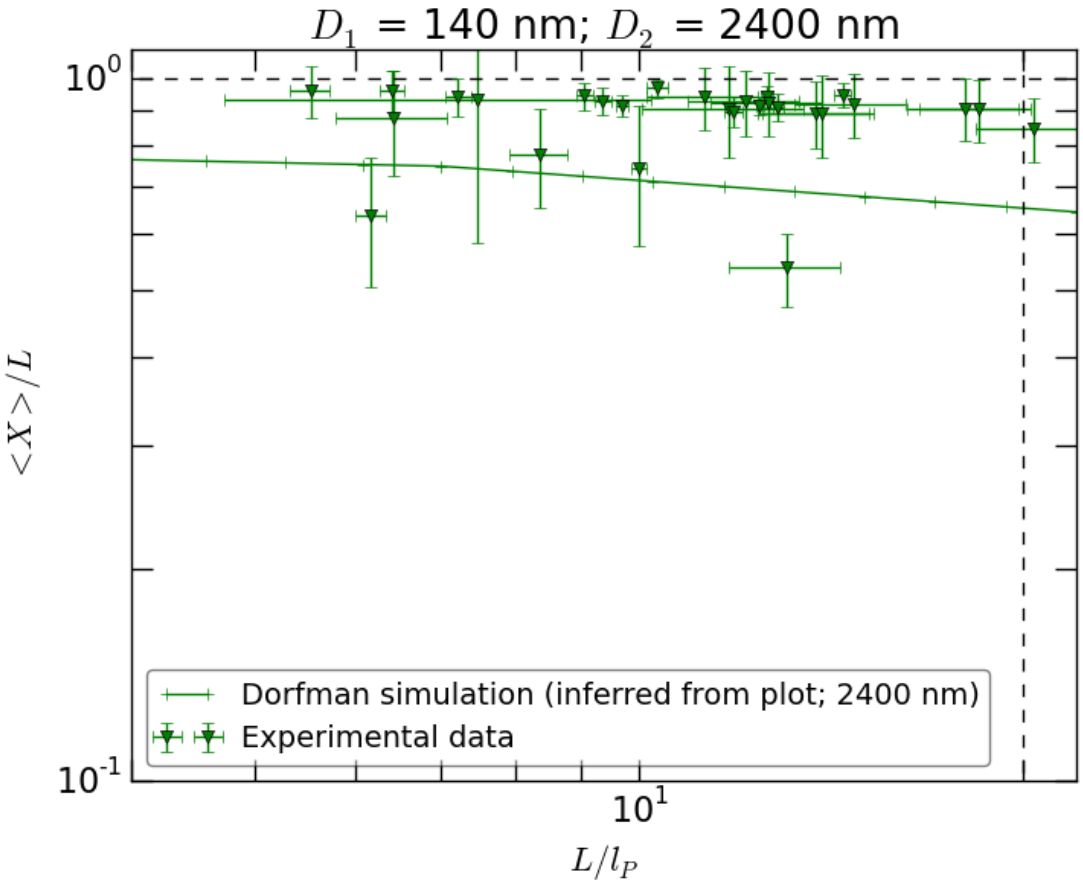


Figure 13: 2400nm channel; log axes. Points represent experimental data, whilst the line represents the simulated data for the 2400nm channel. The dashed vertical line is the dashed line in 8. Error bars represent one standard deviation of the quantities along each axis. The four lower values are 130607-RecA-T4-wide-4 (at $L/l_P = 8.36$), 130607-RecA-T4-narrow-9 ($L/l_P = 6.16$), 130607-RecA-T4-narrow-10 ($L/l_P = 10.00$), and 130905-RecA-T4-narrow-7 ($L/l_P = 13.05$); they were discussed above.

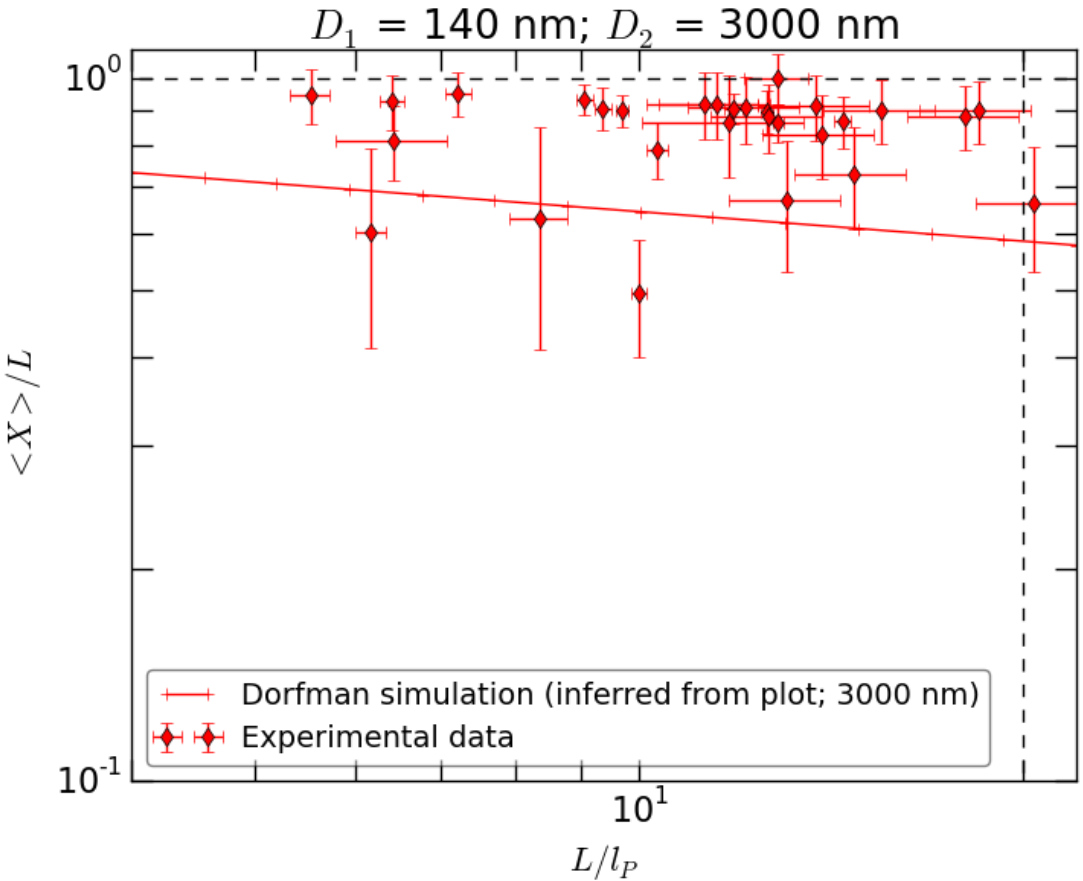


Figure 14: 3000nm channel; log axes. Points represent experimental data, whilst the line represents the simulated data for the 3000nm channel. The dashed vertical line is the dashed line in 8. Error bars represent one standard deviation of the quantities along each axis. The five lower values are 130607-RecA-T4-wide-4 (at $L/l_P = 8.36$), 130607-RecA-T4-narrow-9 ($L/l_P = 6.16$), 130607-RecA-T4-narrow-10 ($L/l_P = 10.00$), and 130905-RecA-T4-narrow-7 ($L/l_P = 13.05$), as well as 130924-RecA-lambda-wide2 ($L/l_P = 20.37$); these were discussed above.

2.2 T4 results

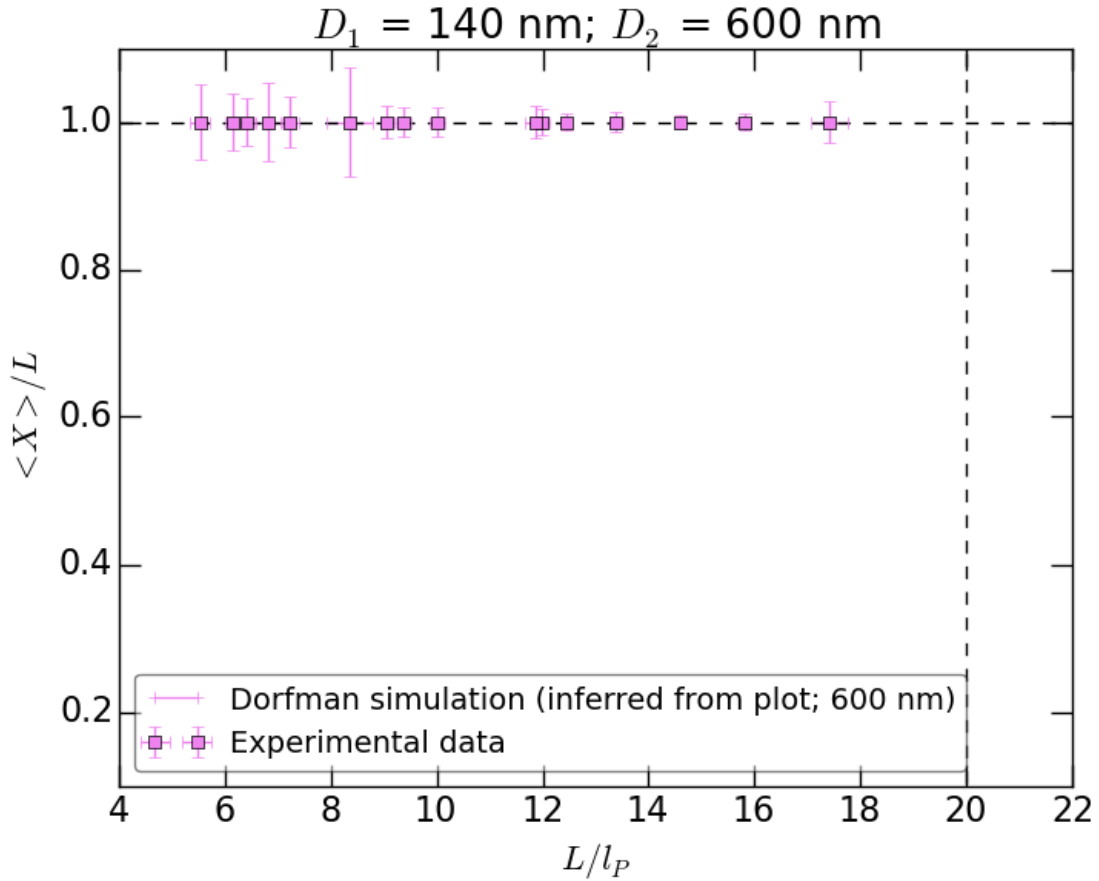


Figure 15: 600nm channel; linear axes. Points represent experimental data, whilst the line represents the simulated data for the 600nm channel. The dashed vertical line is the dashed line in 8. Error bars represent one standard deviation of the quantities along each axis.

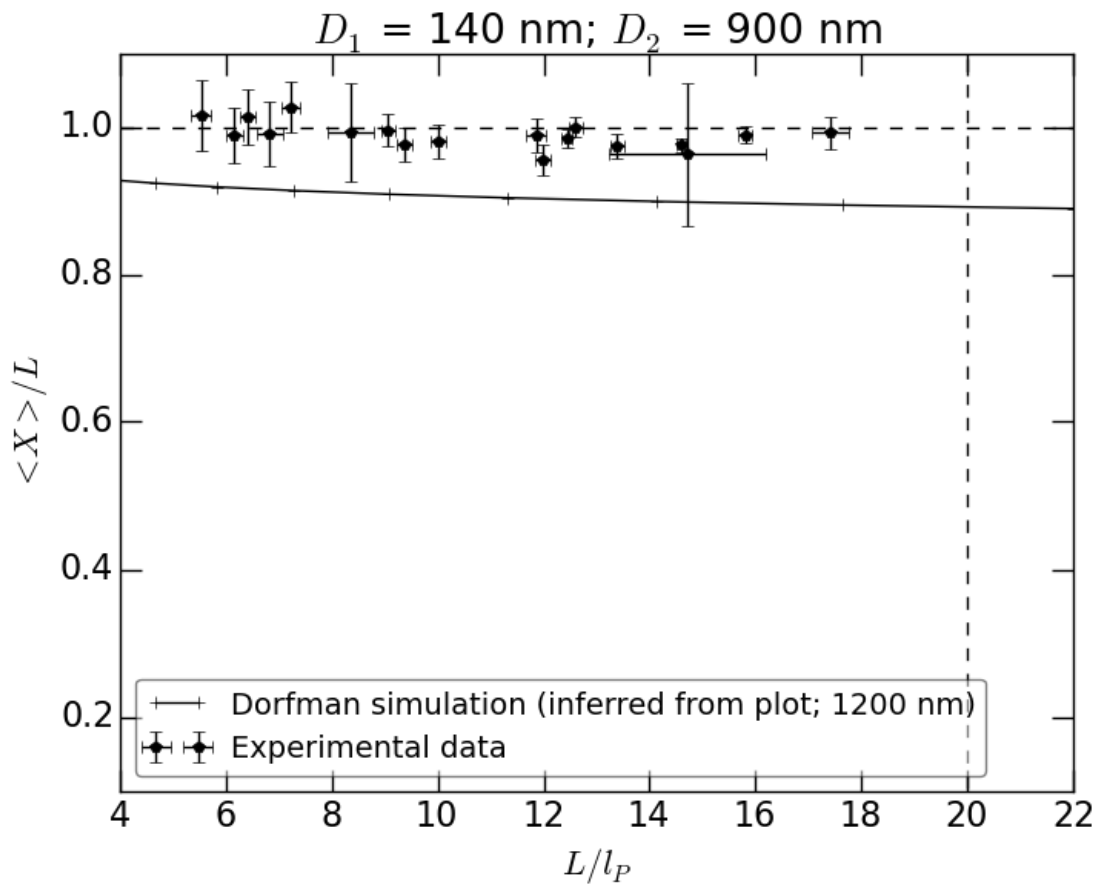


Figure 16: 900nm channel; linear axes. Points represent experimental data, whilst the line represents the simulated data for the 1200nm channel. The dashed vertical line is the dashed line in 8. Error bars represent one standard deviation of the quantities along each axis.

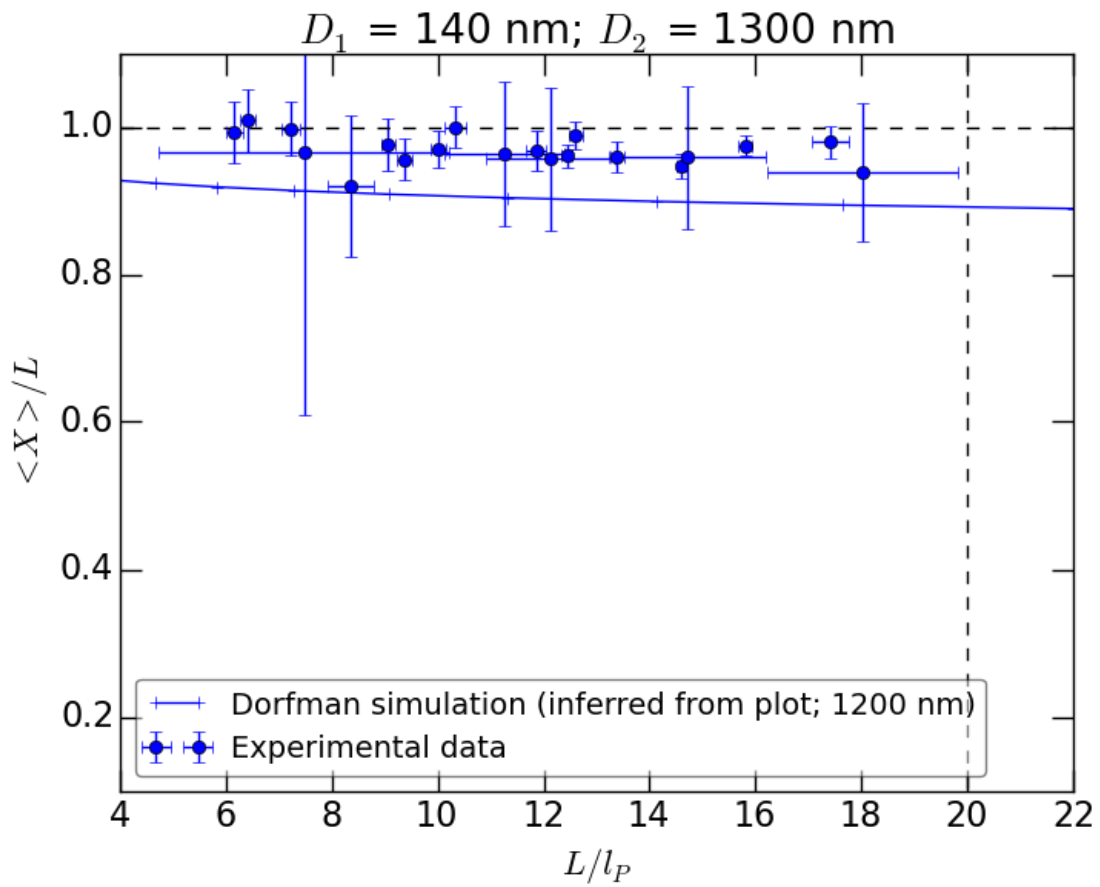


Figure 17: 1300nm channel; linear axes. Points represent experimental data, whilst the line represents the simulated data for the 1200nm channel. The dashed vertical line is the dashed line in 8. Error bars represent one standard deviation of the quantities along each axis.

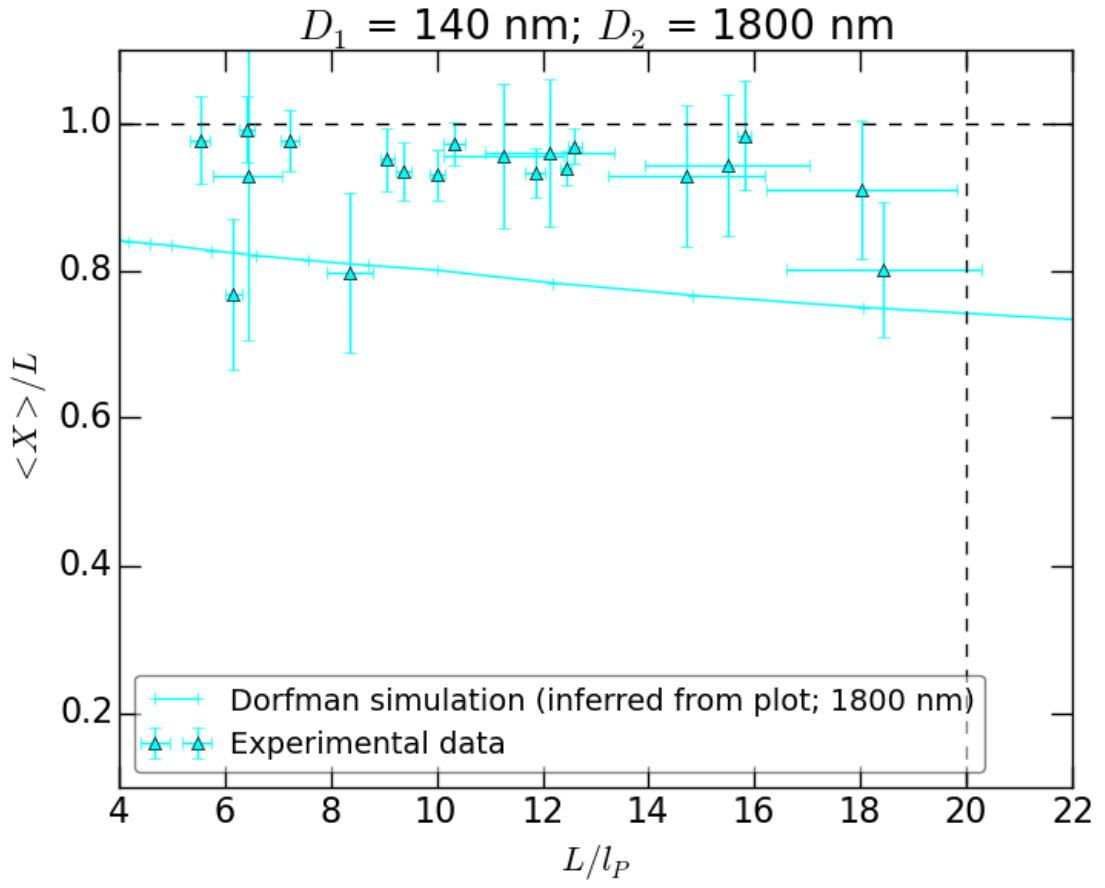


Figure 18: 1800nm channel; linear axes. Points represent experimental data, whilst the line represents the simulated data for the 1800nm channel. The dashed vertical line is the dashed line in 8. Error bars represent one standard deviation of the quantities along each axis. The two lower values are 130607-RecA-T4-wide-4 (at $L/l_P = 8.36$), 130607-RecA-T4-narrow-9 ($L/l_P = 6.16$); these were discussed above.

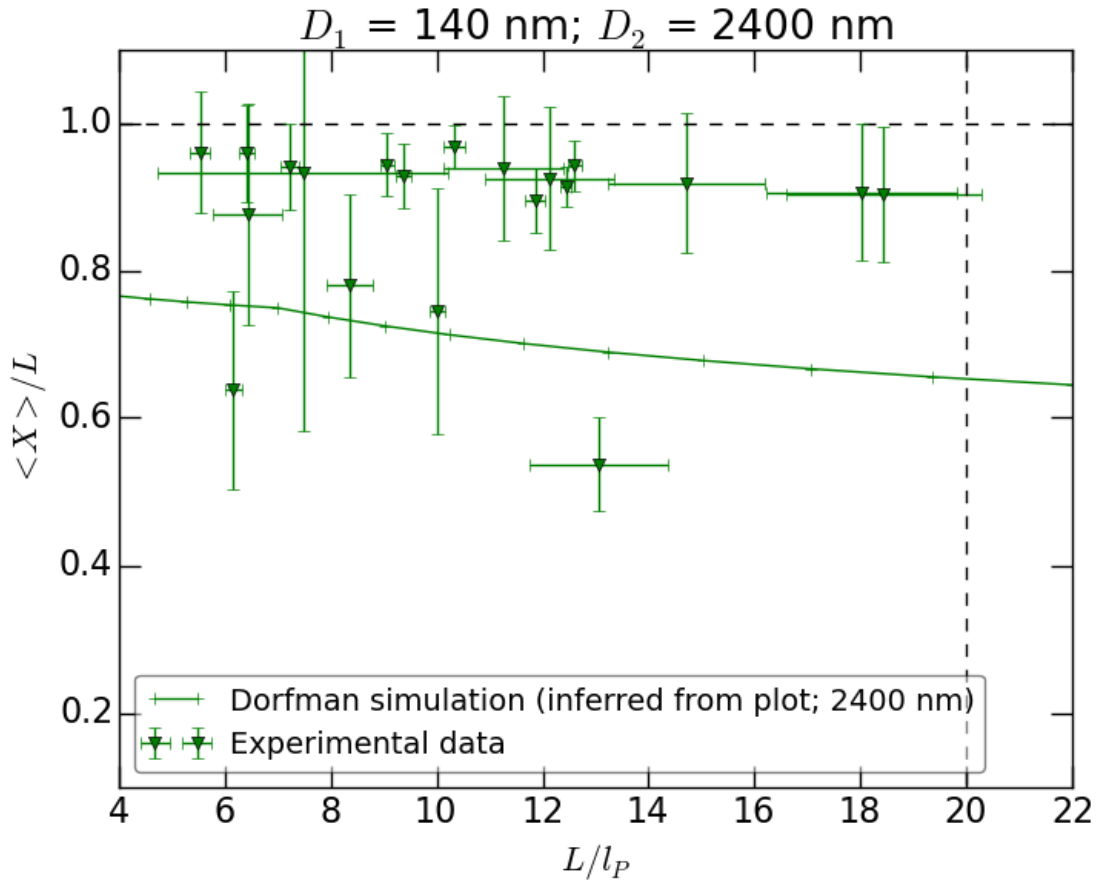


Figure 19: 2400nm channel; linear axes. Points represent experimental data, whilst the line represents the simulated data for the 2400nm channel. The dashed vertical line is the dashed line in 8. Error bars represent one standard deviation of the quantities along each axis. The four lower values are 130607-RecA-T4-wide-4 (at $L/l_P = 8.36$), 130607-RecA-T4-narrow-9 ($L/l_P = 6.16$), 130607-RecA-T4-narrow-10 ($L/l_P = 10.00$), and 130905-RecA-T4-narrow-7 ($L/l_P = 13.05$); they were discussed above.

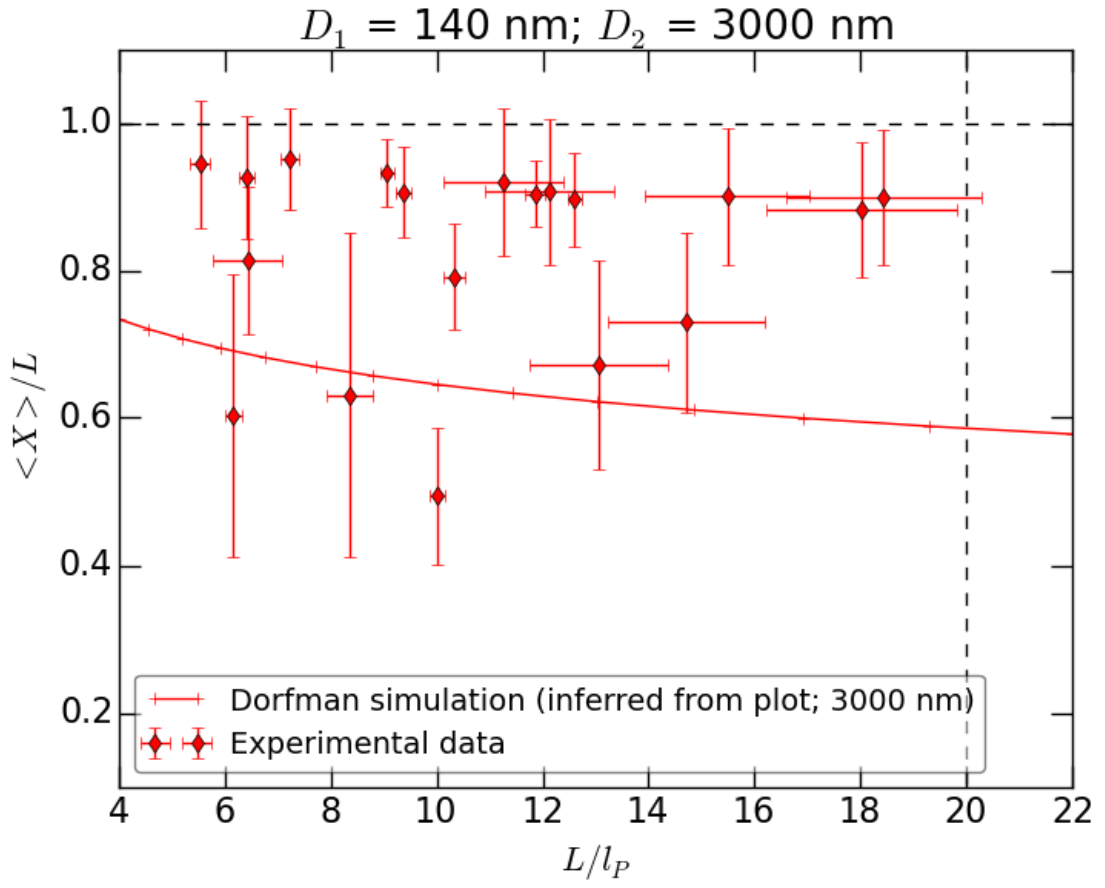


Figure 20: 3000nm channel; linear axes. Points represent experimental data, whilst the line represents the simulated data for the 3000nm channel. The dashed vertical line is the dashed line in 8. Error bars represent one standard deviation of the quantities along each axis. The four lower values are 130607-RecA-T4-wide-4 (at $L/l_P = 8.36$), 130607-RecA-T4-narrow-9 ($L/l_P = 6.16$), 130607-RecA-T4-narrow-10 ($L/l_P = 10.00$), and 130905-RecA-T4-narrow-7 ($L/l_P = 13.05$); these were discussed above.

2.3 λ results

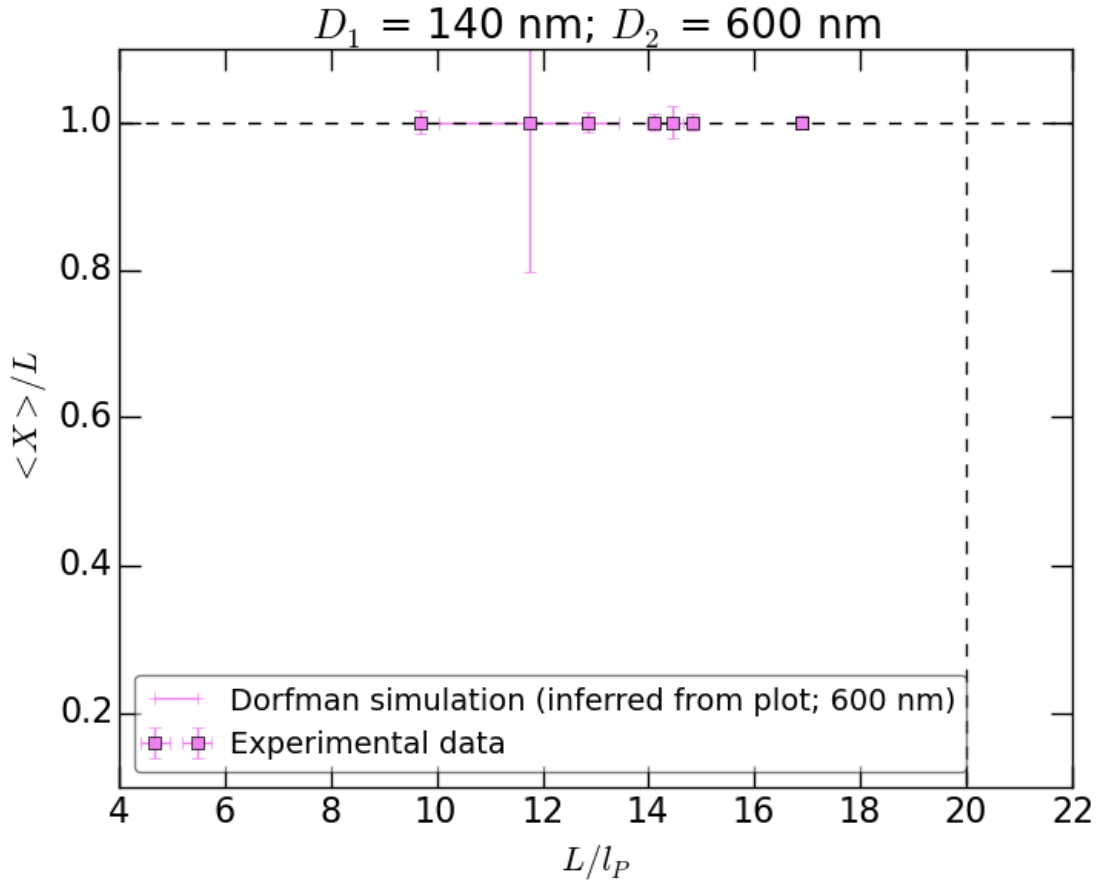


Figure 21: 600nm channel; linear axes. Points represent experimental data, whilst the line represents the simulated data for the 600nm channel. The dashed vertical line is the dashed line in 8. Error bars represent one standard deviation of the quantities along each axis.

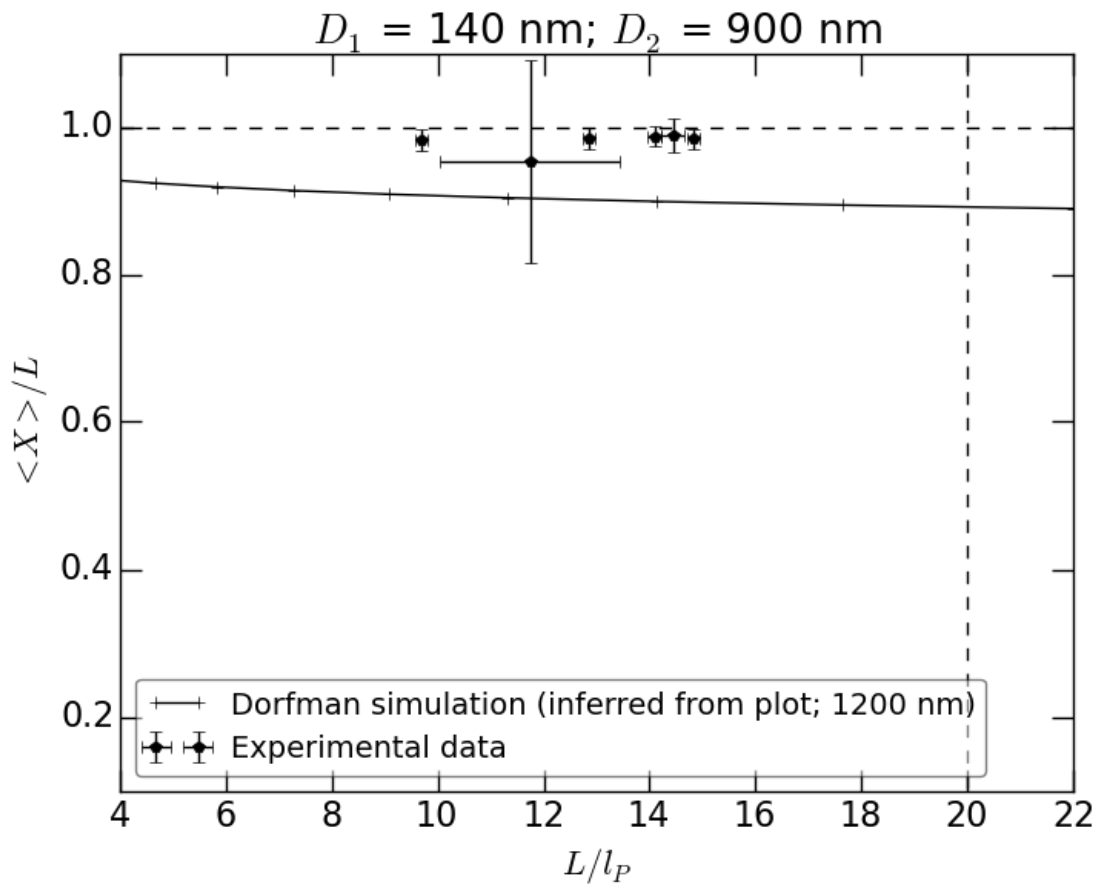


Figure 22: 900nm channel; linear axes. Points represent experimental data, whilst the line represents the simulated data for the 1200nm channel. The dashed vertical line is the dashed line in 8. Error bars represent one standard deviation of the quantities along each axis.

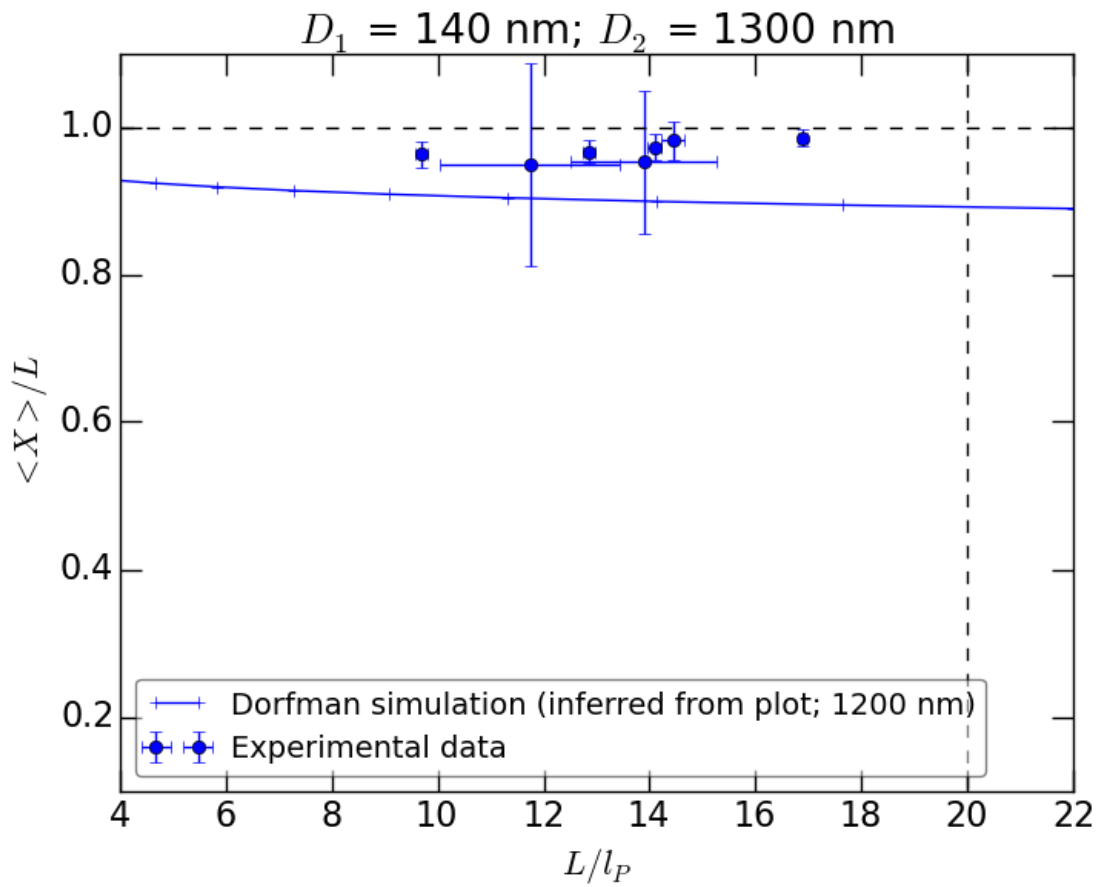


Figure 23: 1300nm channel; linear axes. Points represent experimental data, whilst the line represents the simulated data for the 1200nm channel. The dashed vertical line is the dashed line in 8. Error bars represent one standard deviation of the quantities along each axis.

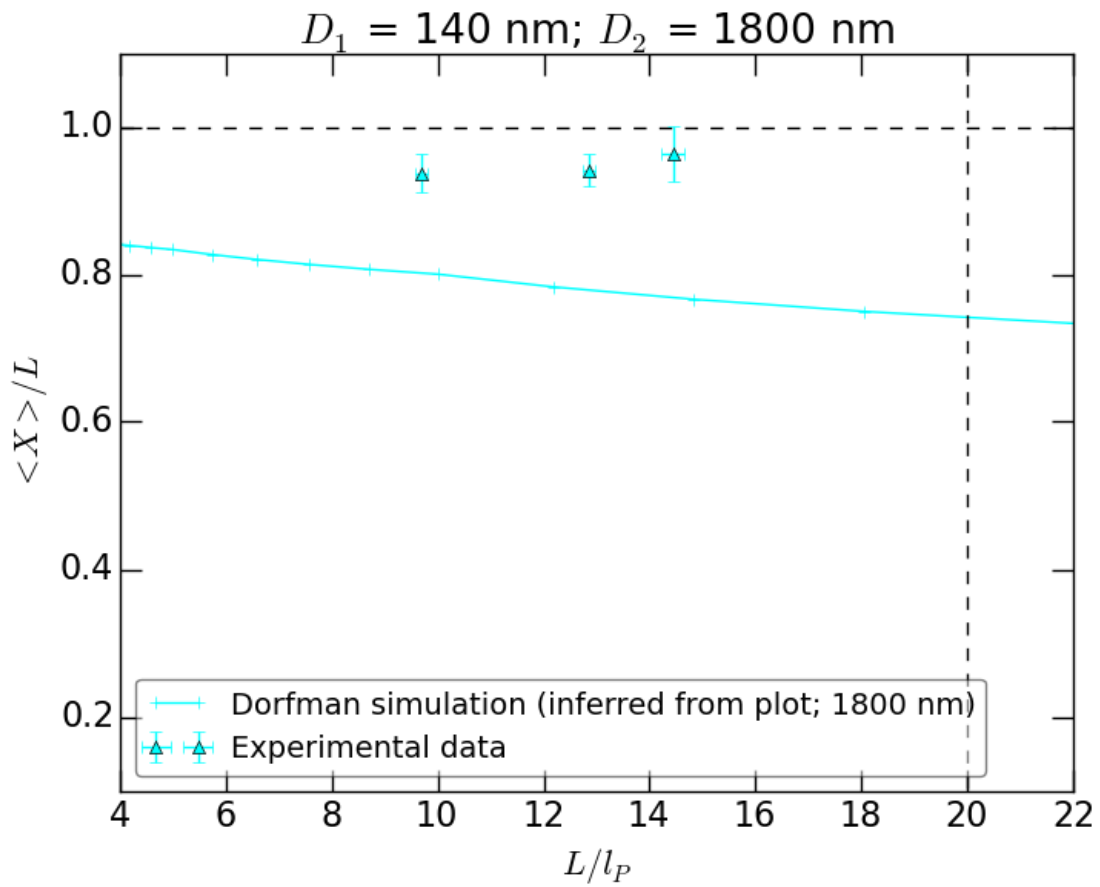


Figure 24: 1800nm channel; linear axes. Points represent experimental data, whilst the line represents the simulated data for the 1800nm channel. The dashed vertical line is the dashed line in 8. Error bars represent one standard deviation of the quantities along each axis.

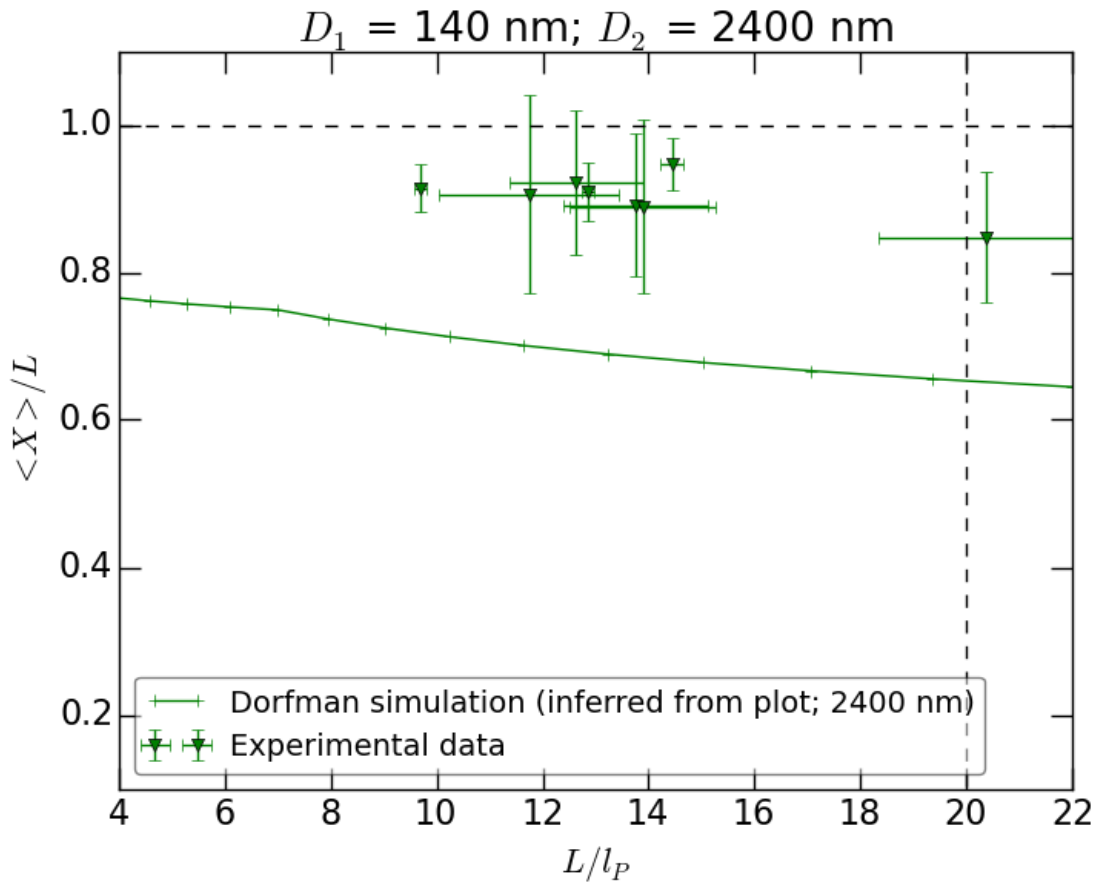


Figure 25: 2400nm channel; linear axes. Points represent experimental data, whilst the line represents the simulated data for the 2400nm channel. The dashed vertical line is the dashed line in 8. Error bars represent one standard deviation of the quantities along each axis. The outlier value is 130924-RecA-lambda-wide-2 ($L/l_P = 20.37$), which was discussed above.

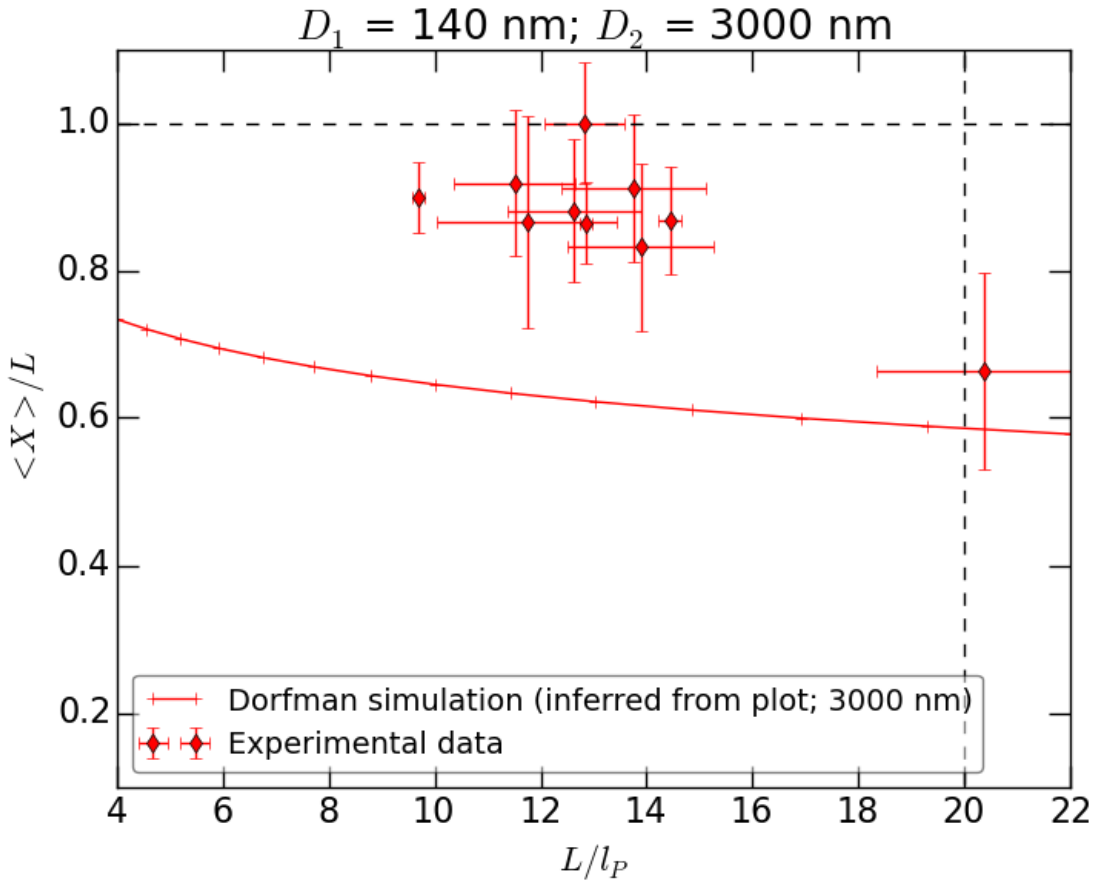


Figure 26: 3000nm channel; linear axes. Points represent experimental data, whilst the line represents the simulated data for the 3000nm channel. The dashed vertical line is the dashed line in 8. Error bars represent one standard deviation of the quantities along each axis. The outlier value is 130924-RecA-lambda-wide-2 ($L/l_P = 20.37$), which was discussed above.

2.4 Rejected configurations

130607-RecA-T4-narrow-8 ($L/l_P = 12.0$) is folded over or knotted at the beginning of the 1300nm sequence, and never unfolds throughout the rest of the experiment. It seems highly likely that this is an experimental error, as there is little change in the conformation from this point on, and its $\langle X \rangle / L$ value (0.52) is a far outlier (not shown). The error can arise when the molecule transitions between channels of different widths, getting tangled in the process; in the experiments tagged ‘narrow’, the molecules start at the narrowest channel, moving to wider channels, whilst in those experiments tagged ‘wide’, the reverse occurs. Once a molecule becomes tangled in this way, it often does not untangle at any point in the rest of the experiment.

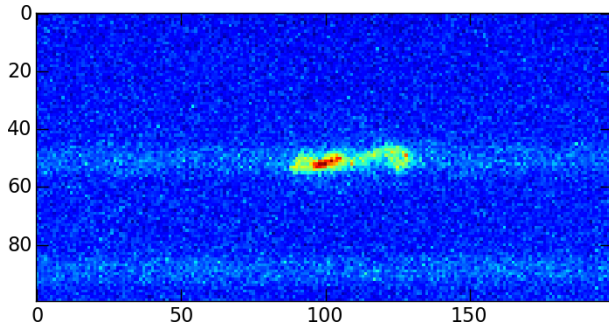


Figure 27: 130607-RecA-T4-narrow-8 at the start of the 1300nm channel sequence

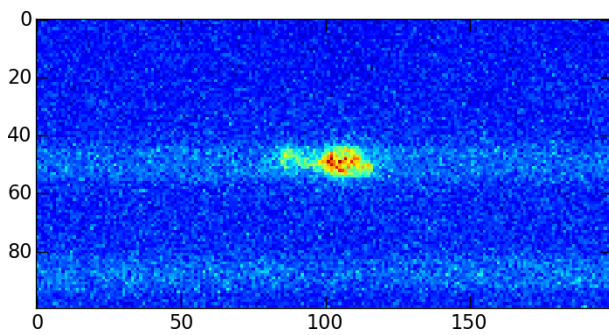


Figure 28: 130607-RecA-T4-narrow-8 at the start of the 1800nm channel sequence

Similarly suspicious experimental conditions are visible in the following cases: 130905-RecA-T4-narrow-3 (1800nm), 130905-RecA-T4-narrow-4 (1800nm), 130905-RecA-T4-wide-3 (600nm and 900nm), 130905-RecA-T4-wide-7 (600nm), 130905-RecA-T4-wide-8 (1300nm), and 130924-RecA-lambda-wide-3 (2400nm).

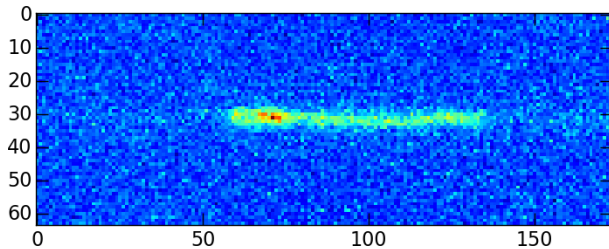


Figure 29: 130605-RecA-T4-wide-7 at the start of the 600nm channel sequence

The following configurations were rejected because their relative L errors exceeded the 0.4 threshold: 130603-RecA-T4-wide-2 (0.52) and 130603-RecA-T4-wide-3 (0.65). The following configurations were rejected because their relative $\langle X \rangle / L$ errors exceeded the 0.4 threshold: 130603-RecA-T4-wide-5 (0.52 at 1800nm, 0.41 at 3000nm); 130607-RecA-T4-wide-1 (0.64 at 1300nm); and 130905-RecA-T4-wide-1 (0.51 at 3000nm).

3 Kymographs

These kymographs were produced by stacking the intensity profiles produced for each sequence of frames as described above.

3.1 130603-RecA-T4-wide-2

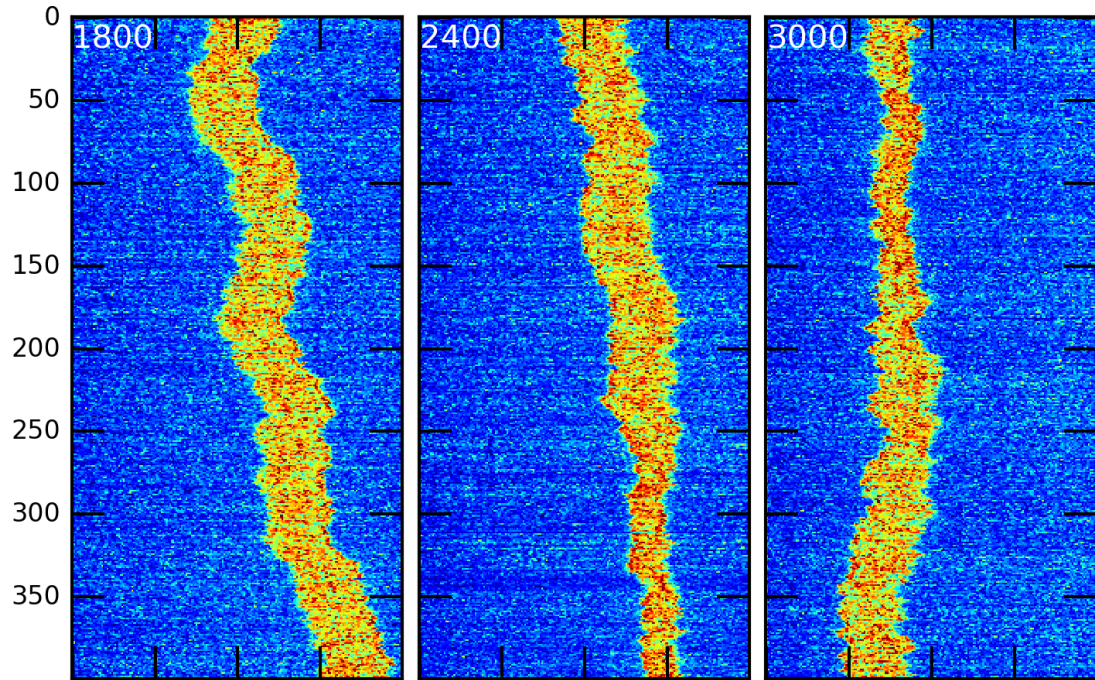


Figure 30: Vertical axis is time. White annotation gives channel width in nanometres.

3.2 130603-RecA-T4-wide-3

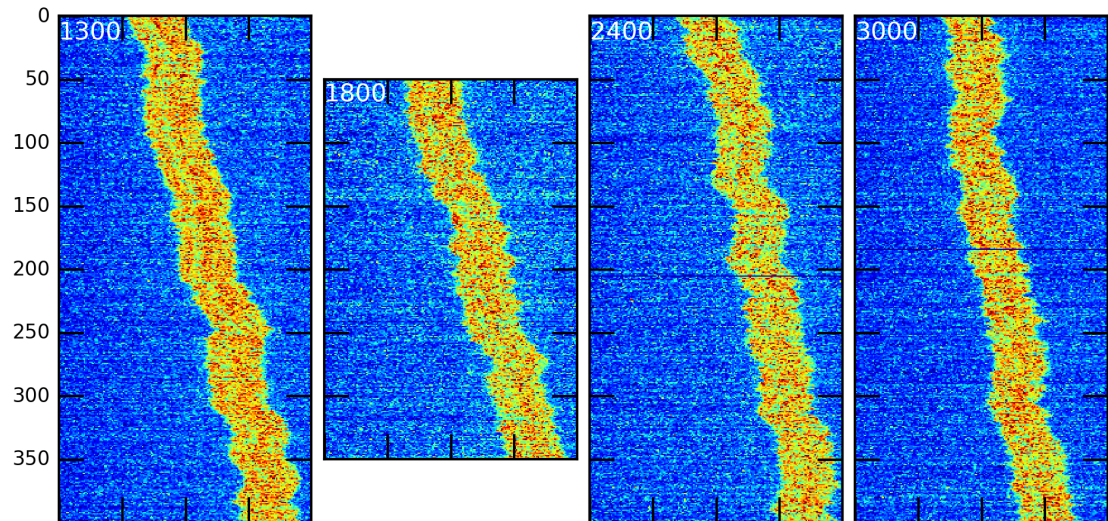


Figure 31: Vertical axis is time. White annotation gives channel width in nanometres.

3.3 130603-RecA-T4-wide-4

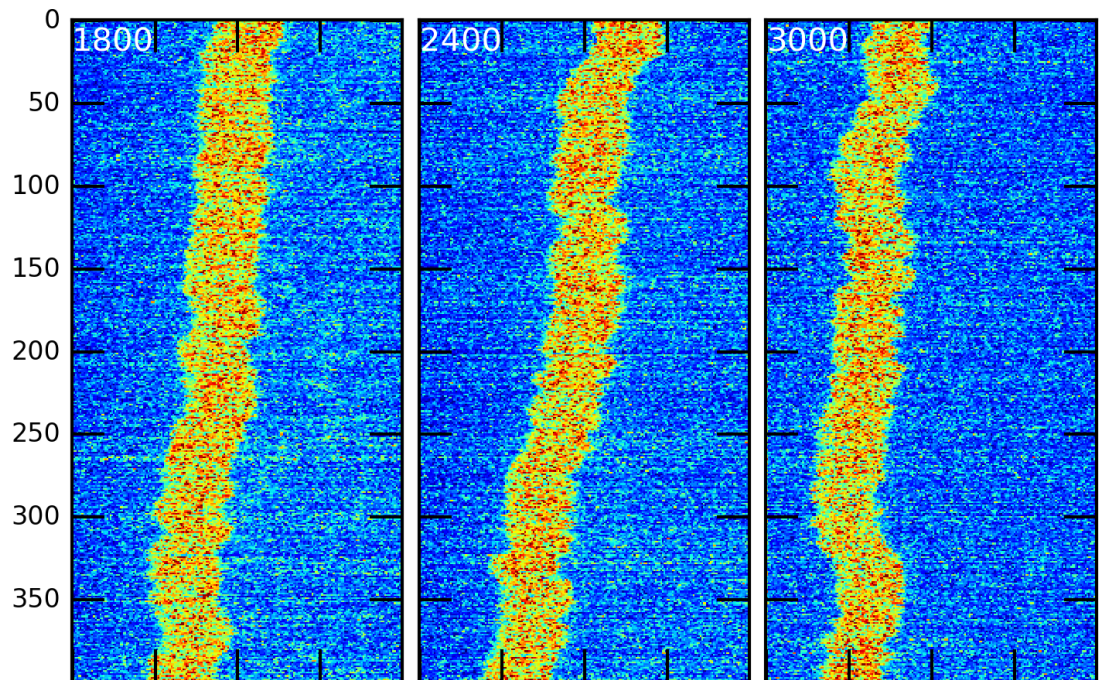


Figure 32: Vertical axis is time. White annotation gives channel width in nanometres.

3.4 130603-RecA-T4-wide-5

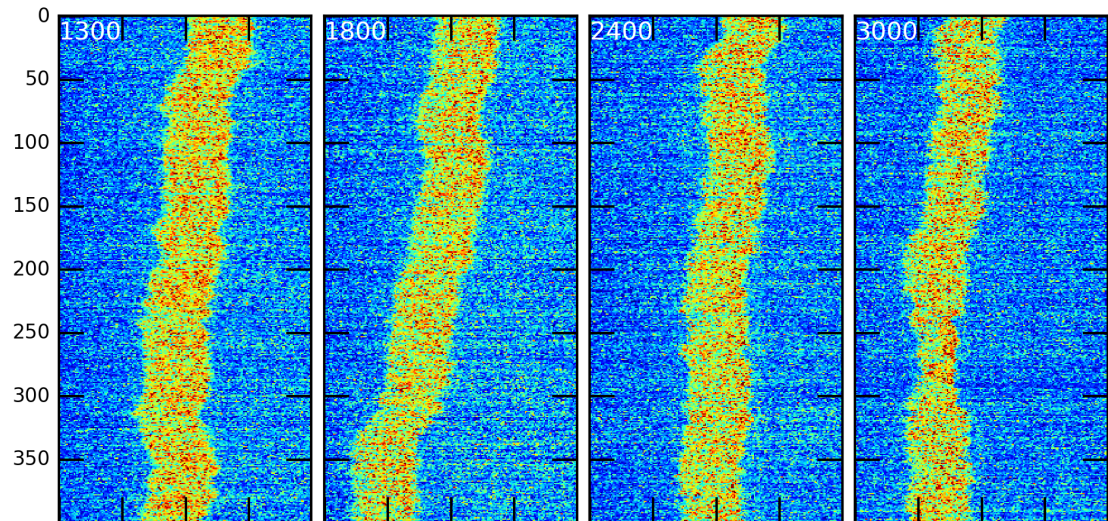


Figure 33: Vertical axis is time. White annotation gives channel width in nanometres.

3.5 130603-RecA-T4-wide-7

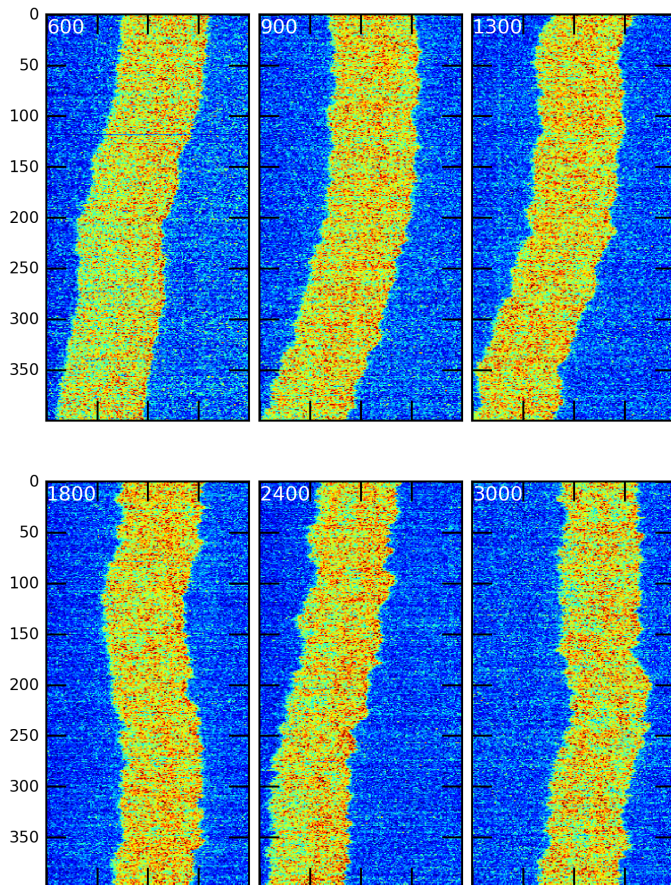


Figure 34: Vertical axis is time. White annotation gives channel width in nanometres.

3.6 130607-RecA-T4-narrow-10

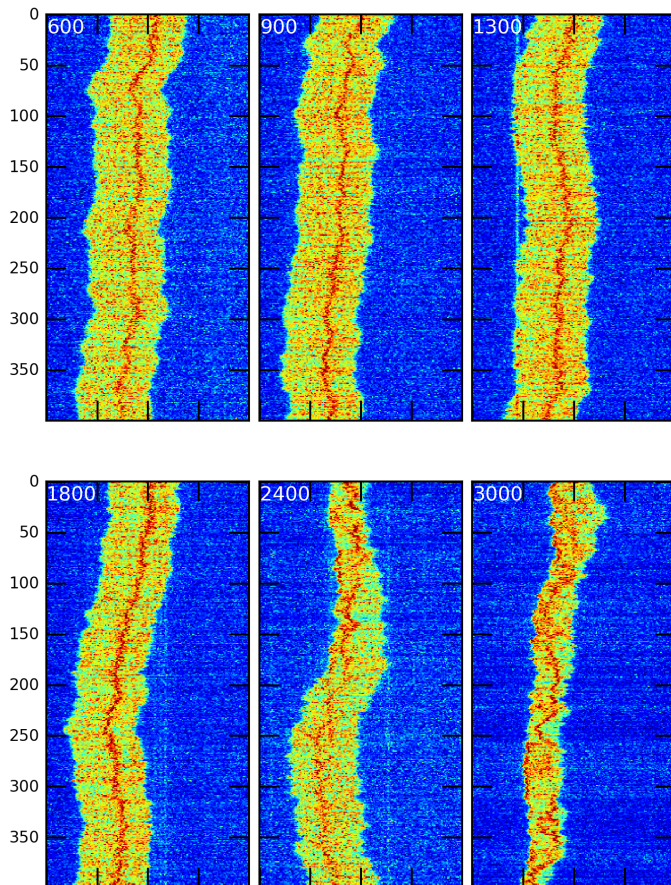


Figure 35: Vertical axis is time. White annotation gives channel width in nanometres.

3.7 130607-RecA-T4-narrow-7

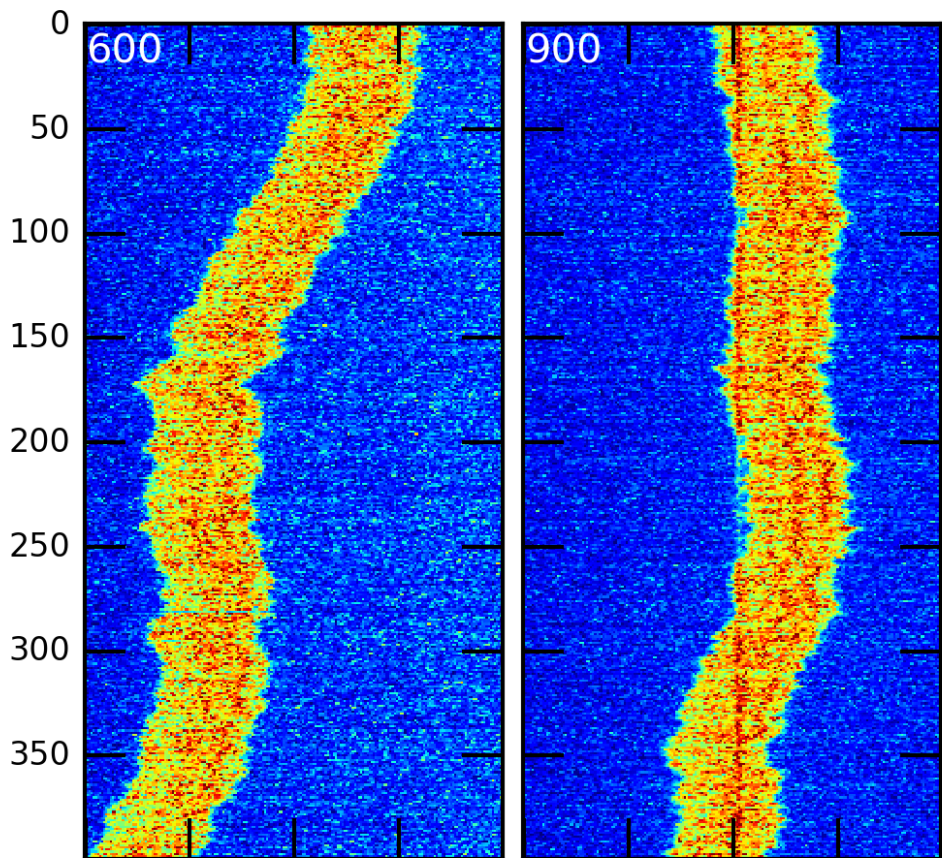


Figure 36: Vertical axis is time. White annotation gives channel width in nanometres.

3.8 130607-RecA-T4-narrow-8

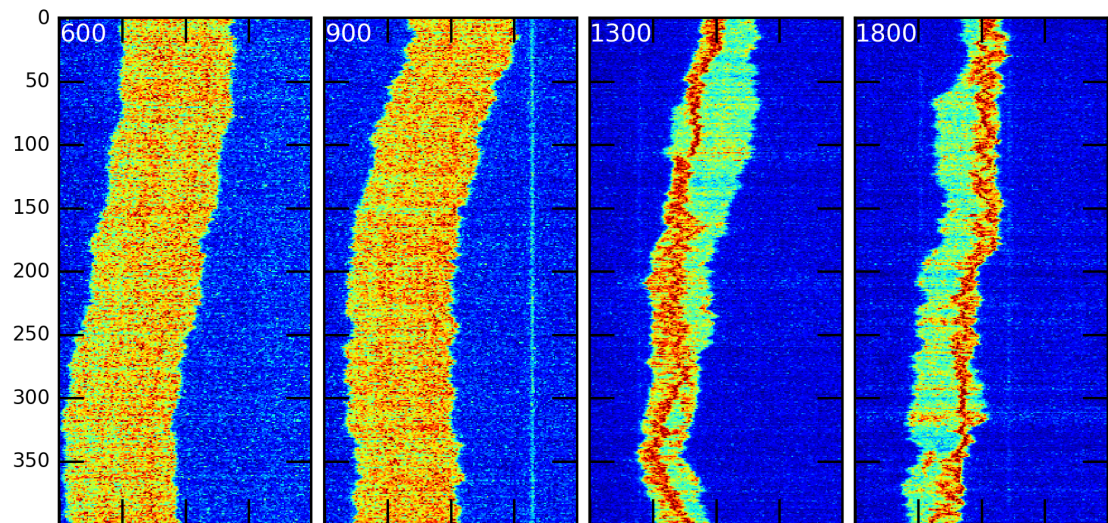


Figure 37: Vertical axis is time. White annotation gives channel width in nanometres.

3.9 130607-RecA-T4-narrow-9

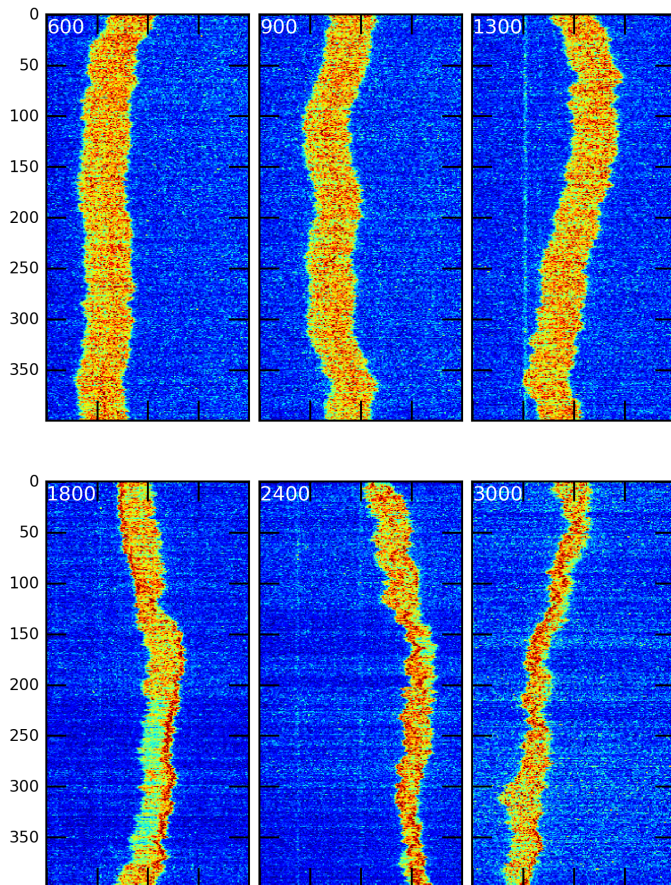


Figure 38: Vertical axis is time. White annotation gives channel width in nanometres.

3.10 130607-RecA-T4-wide-1

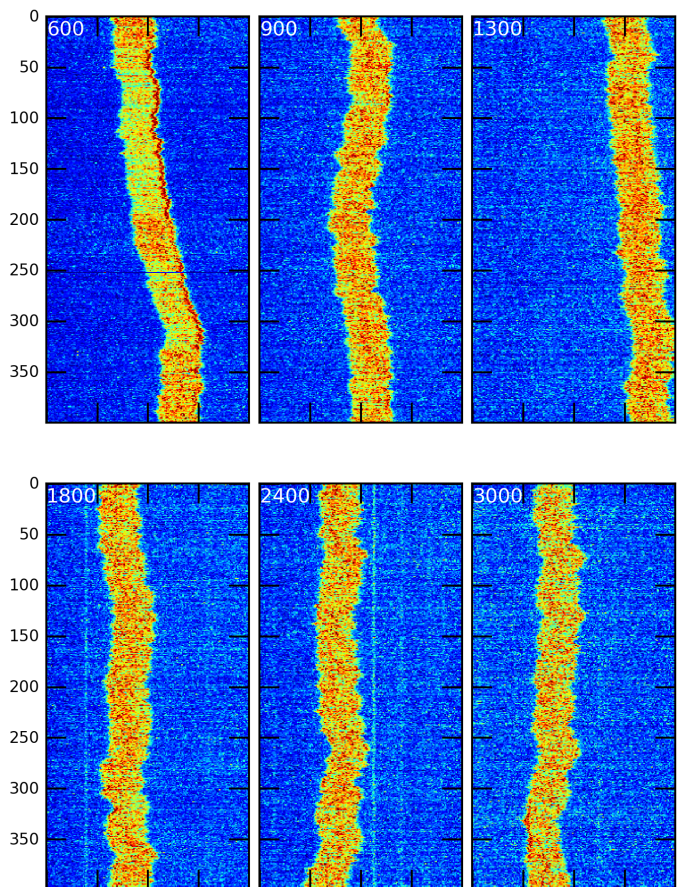


Figure 39: Vertical axis is time. White annotation gives channel width in nanometres.

3.11 130607-RecA-T4-wide-2

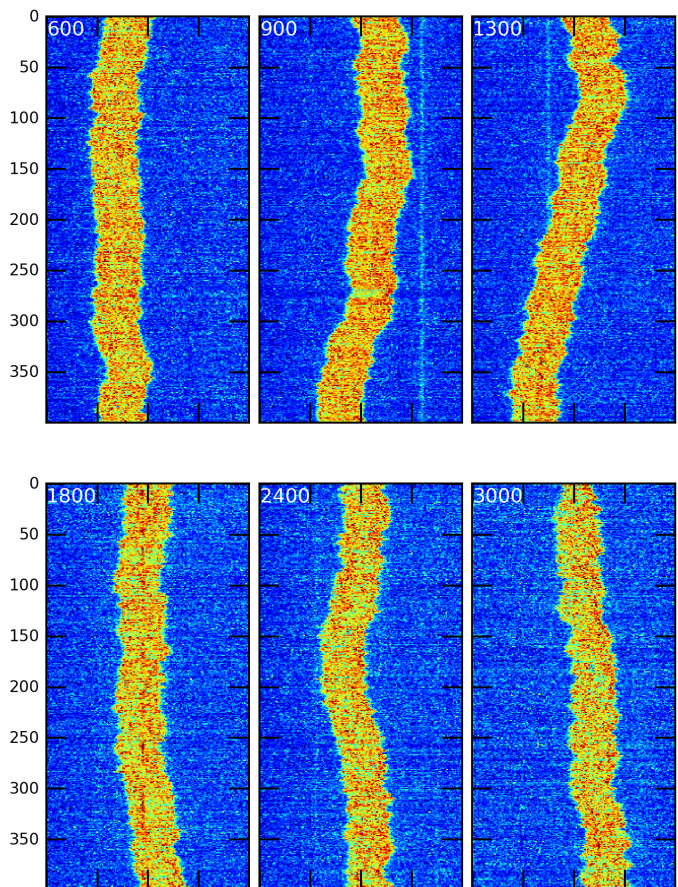


Figure 40: Vertical axis is time. White annotation gives channel width in nanometres.

3.12 130607-RecA-T4-wide-3

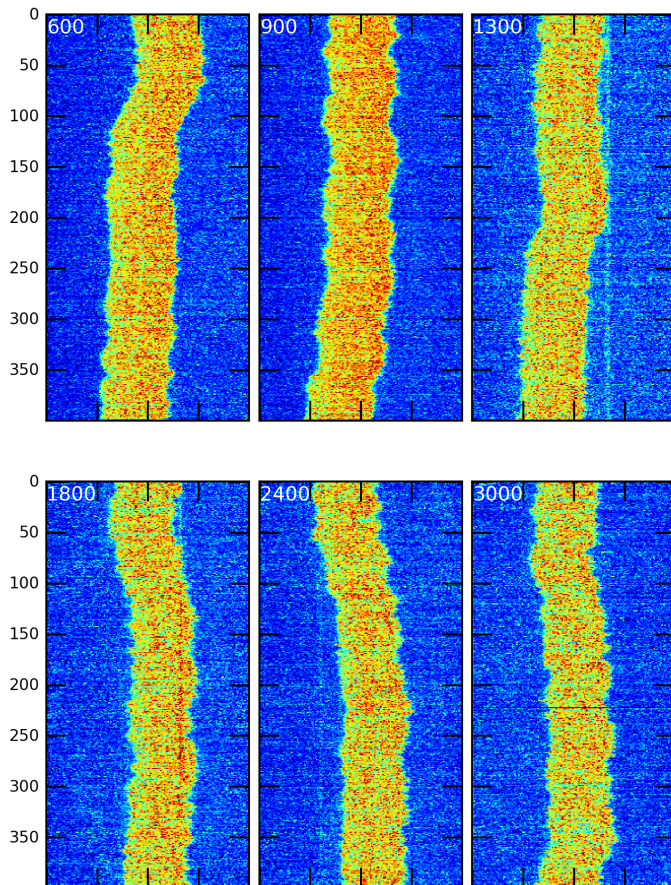


Figure 41: Vertical axis is time. White annotation gives channel width in nanometres.

3.13 130607-RecA-T4-wide-4

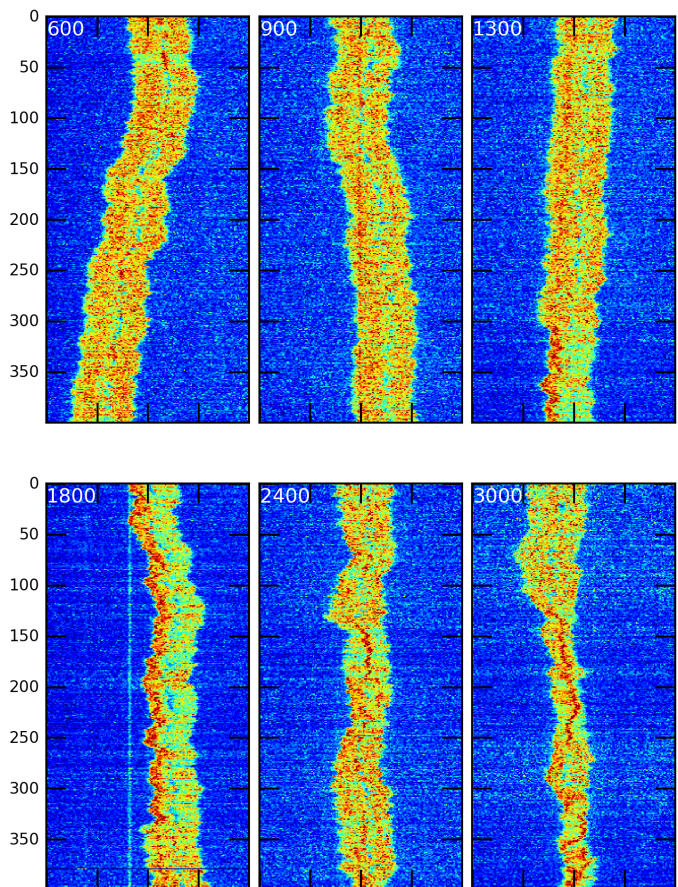


Figure 42: Vertical axis is time. White annotation gives channel width in nanometres.

3.14 130607-RecA-T4-wide-5

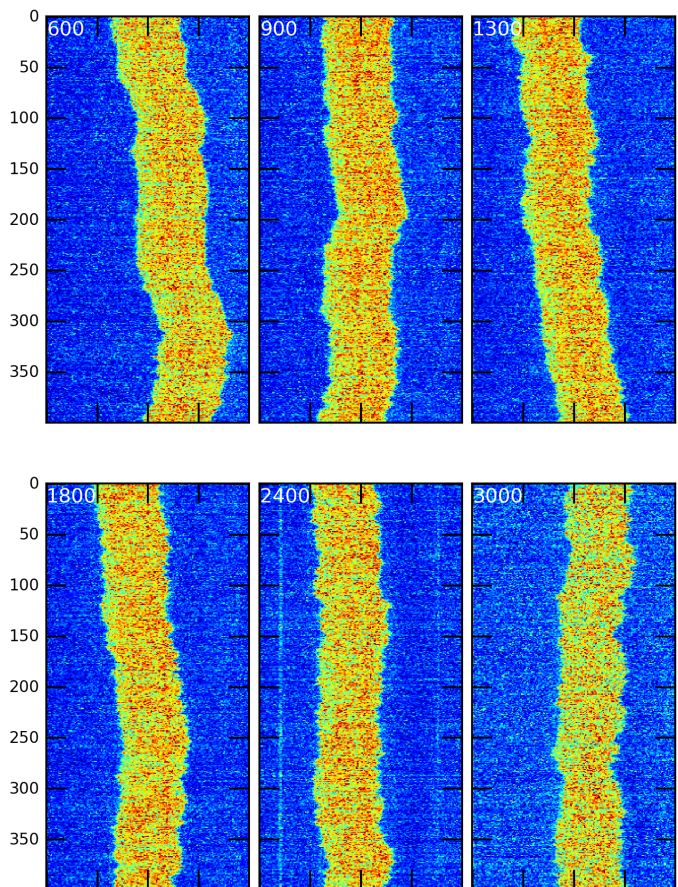


Figure 43: Vertical axis is time. White annotation gives channel width in nanometres.

3.15 130607-RecA-T4-wide-6

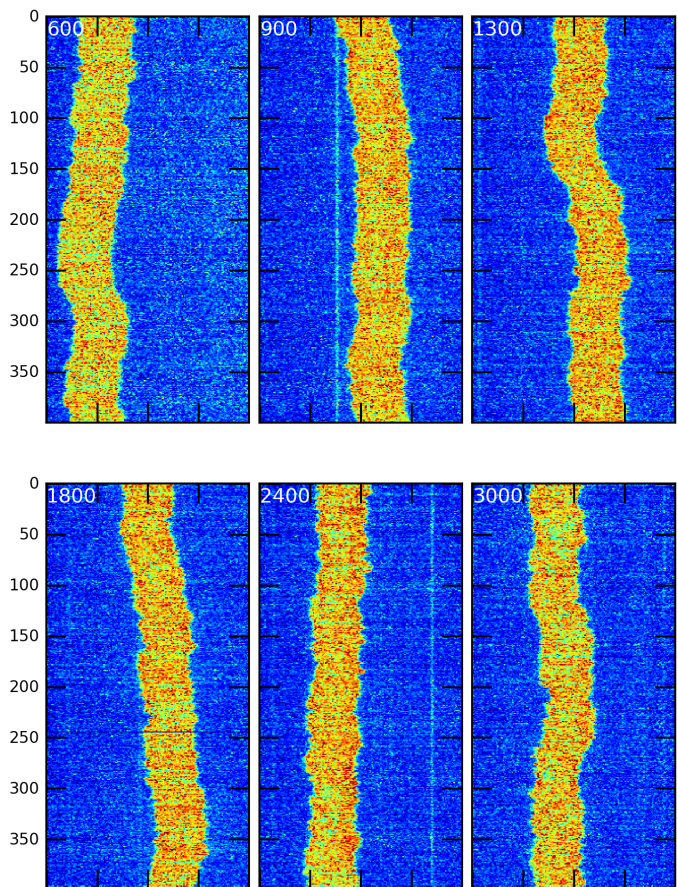


Figure 44: Vertical axis is time. White annotation gives channel width in nanometres.

3.16 130905-RecA-T4-narrow-1

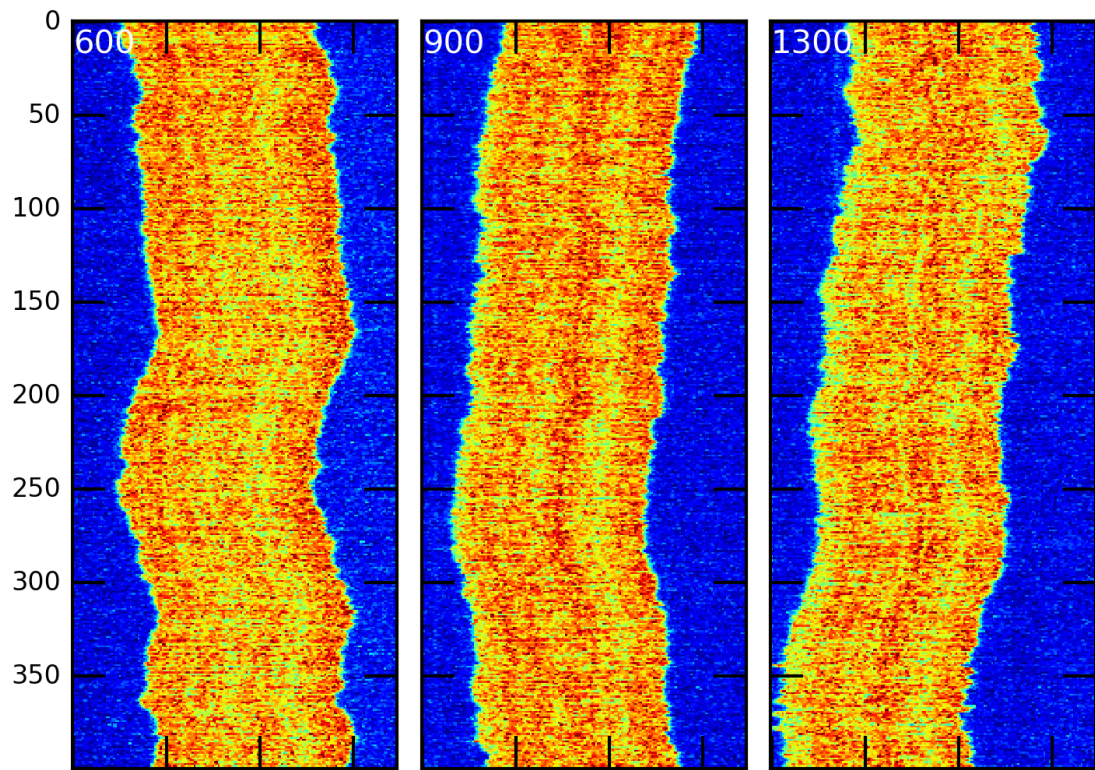


Figure 45: Vertical axis is time. White annotation gives channel width in nanometres.

3.17 130905-RecA-T4-narrow-2

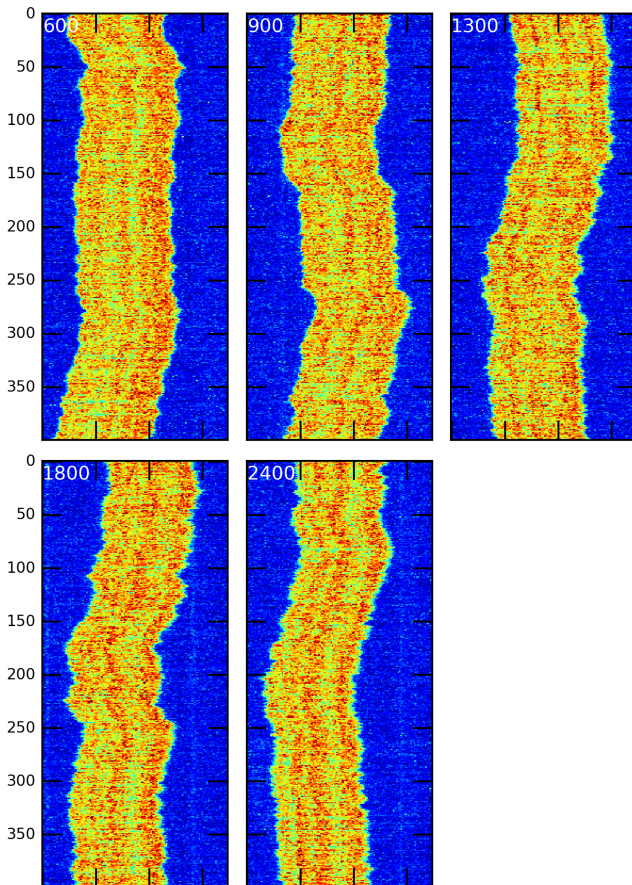


Figure 46: Vertical axis is time. White annotation gives channel width in nanometres.

3.18 130905-RecA-T4-narrow-3

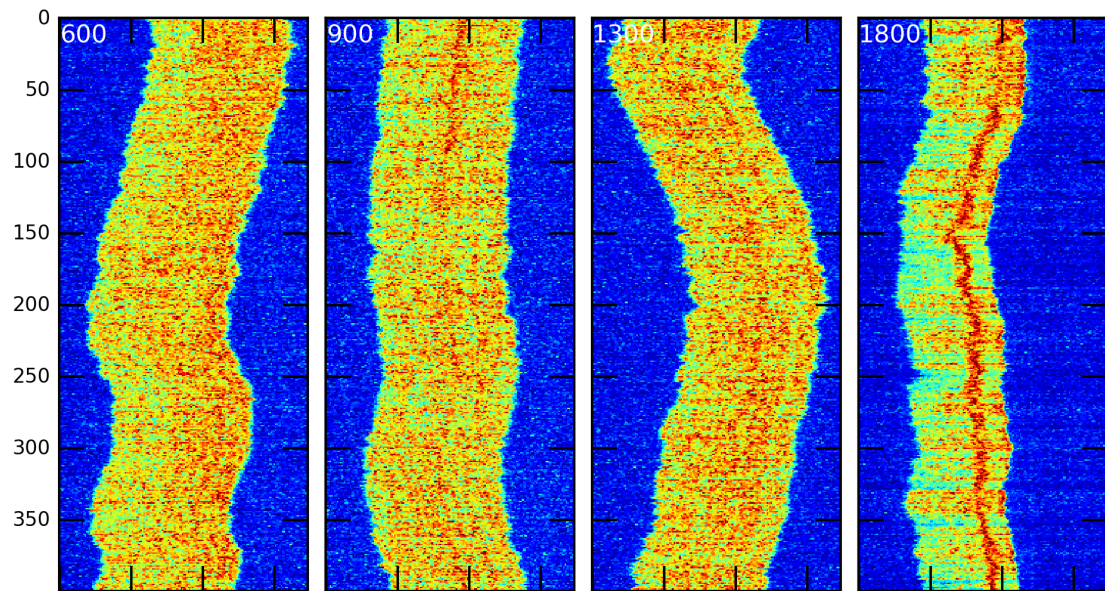


Figure 47: Vertical axis is time. White annotation gives channel width in nanometres.

3.19 130905-RecA-T4-narrow-4

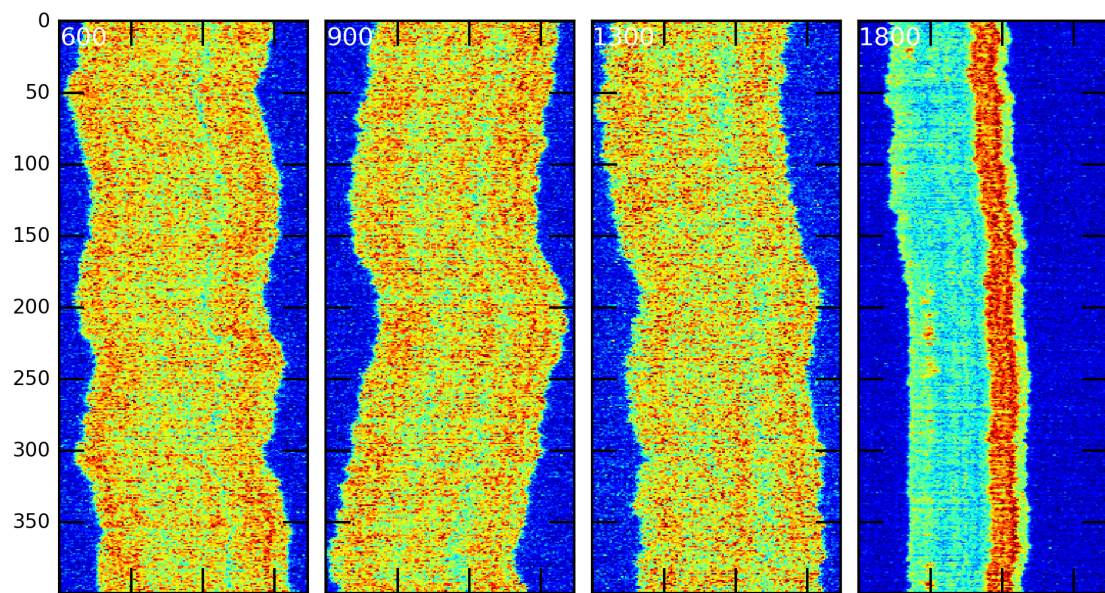


Figure 48: Vertical axis is time. White annotation gives channel width in nanometres.

3.20 130905-RecA-T4-narrow-5

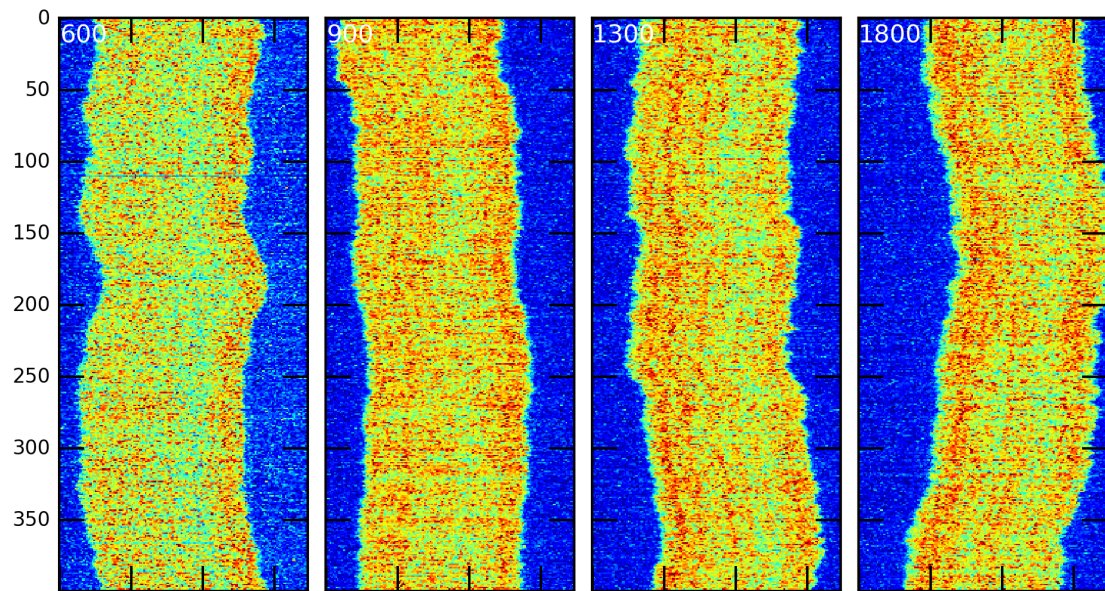


Figure 49: Vertical axis is time. White annotation gives channel width in nanometres.

3.21 130905-RecA-T4-narrow-6

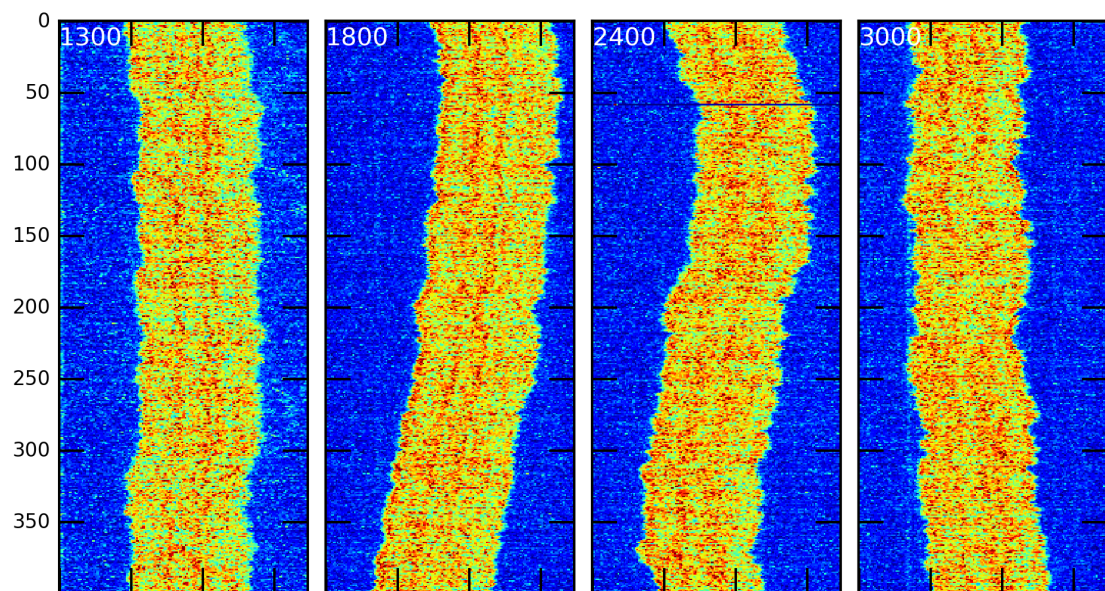


Figure 50: Vertical axis is time. White annotation gives channel width in nanometres.

3.22 130905-RecA-T4-narrow-7

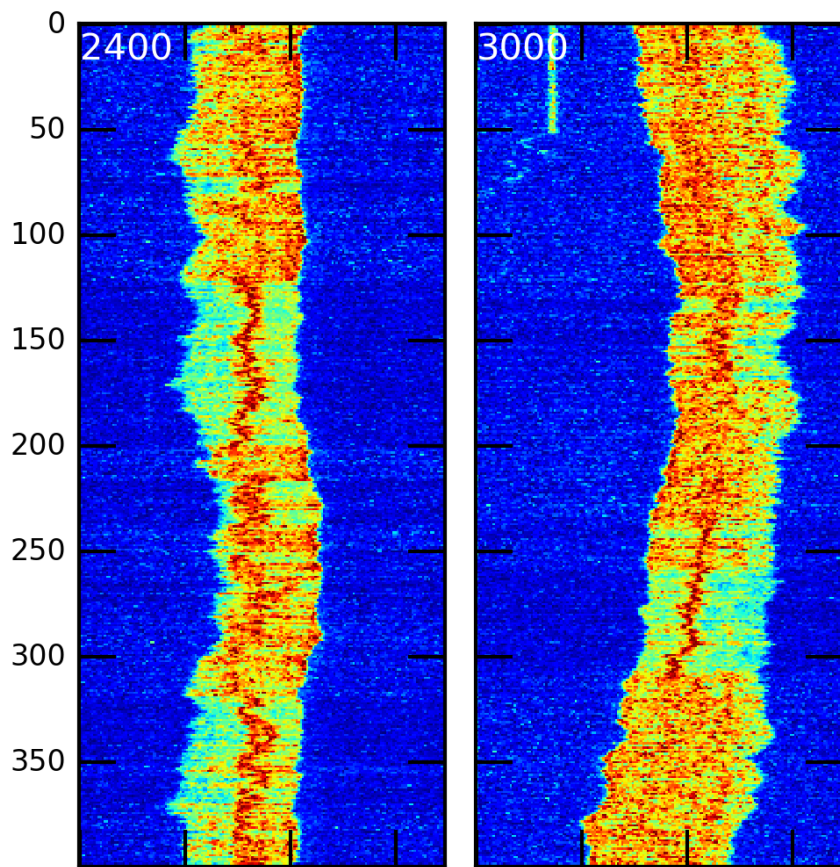


Figure 51: Vertical axis is time. White annotation gives channel width in nanometres.

3.23 130905-RecA-T4-wide-1

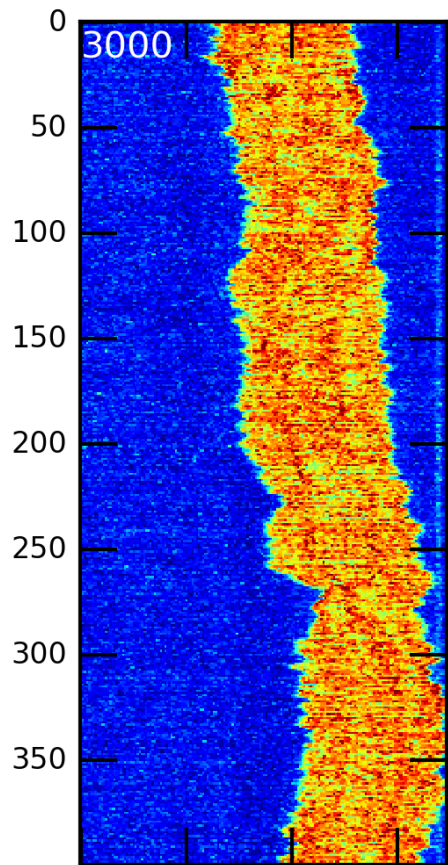


Figure 52: Vertical axis is time. White annotation gives channel width in nanometres.

3.24 130905-RecA-T4-wide-2

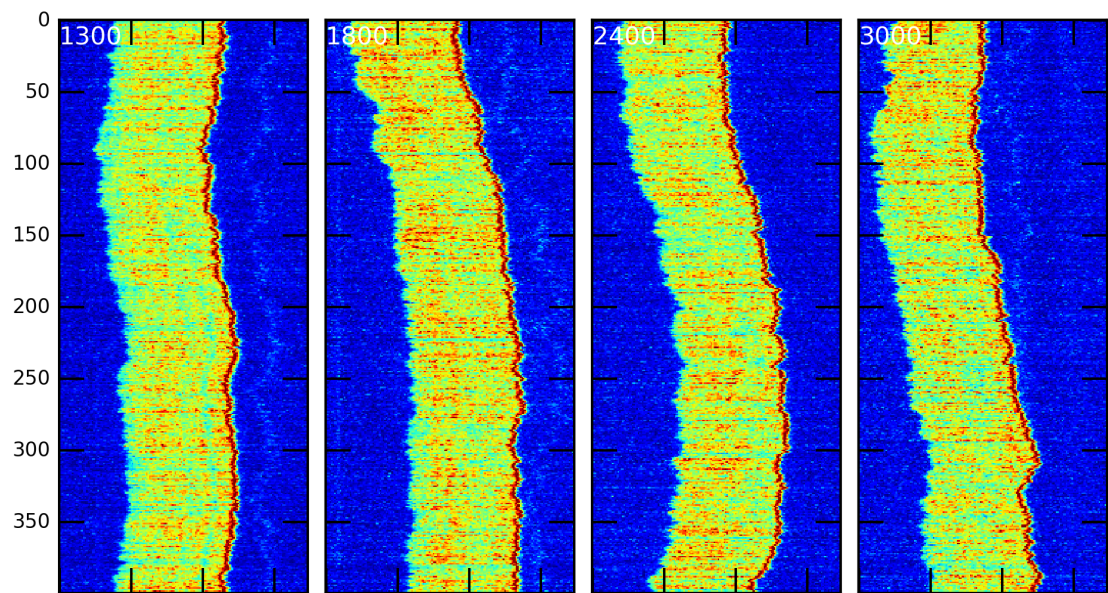


Figure 53: Vertical axis is time. White annotation gives channel width in nanometres.

3.25 130905-RecA-T4-wide-3

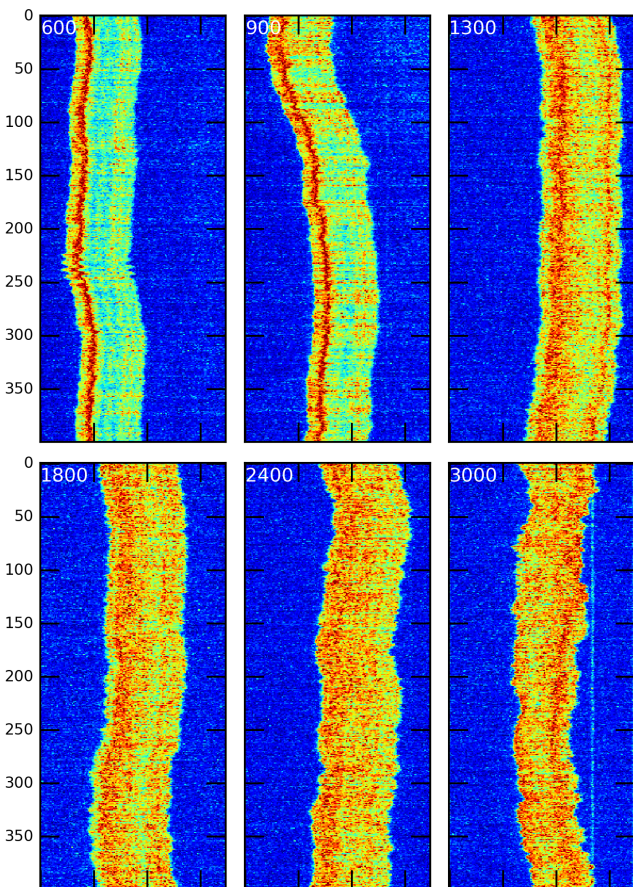


Figure 54: Vertical axis is time. White annotation gives channel width in nanometres.

3.26 130905-RecA-T4-wide-4

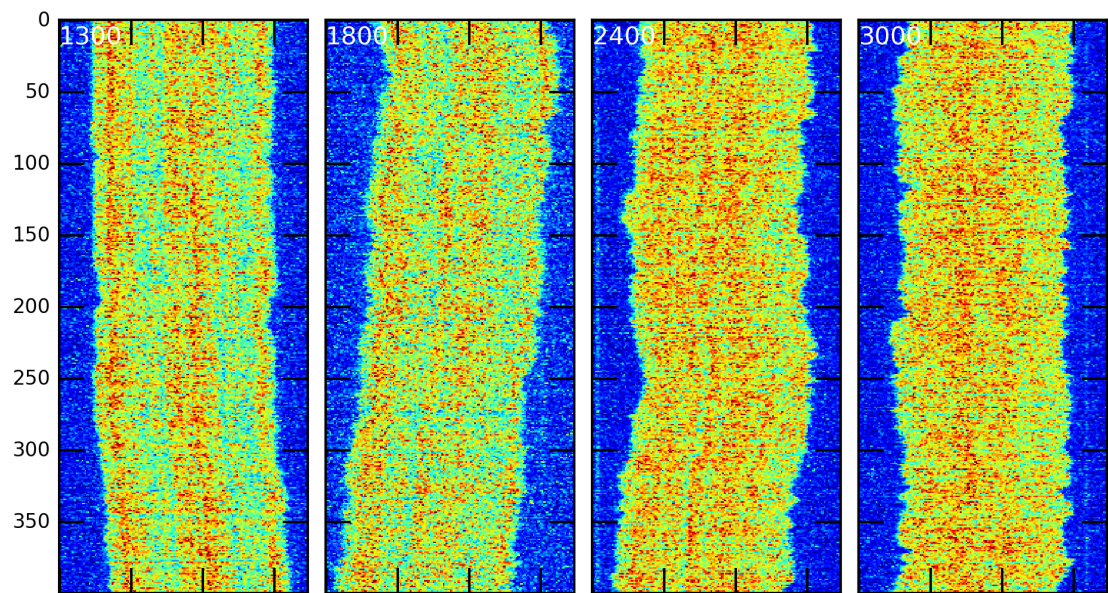


Figure 55: Vertical axis is time. White annotation gives channel width in nanometres.

3.27 130905-RecA-T4-wide-5

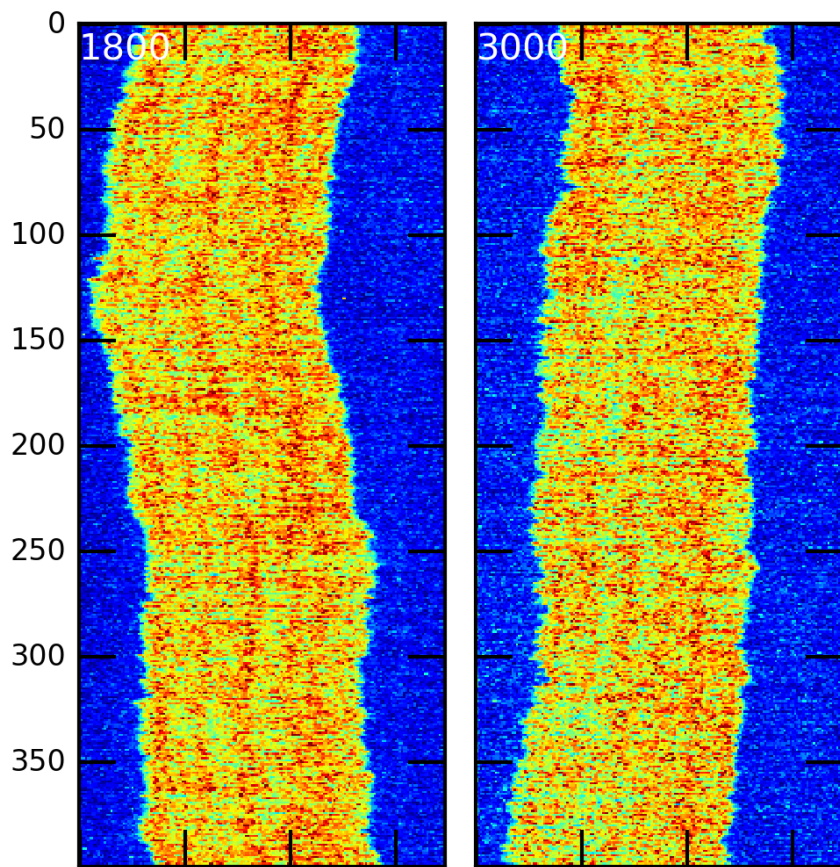


Figure 56: Vertical axis is time. White annotation gives channel width in nanometres.

3.28 130905-RecA-T4-wide-6

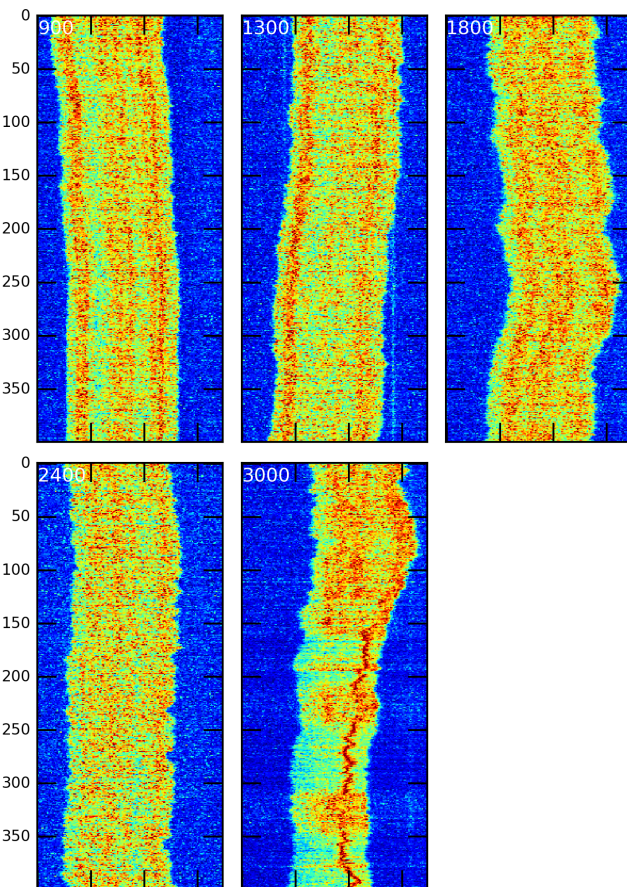


Figure 57: Vertical axis is time. White annotation gives channel width in nanometres.

3.29 130905-RecA-T4-wide-7

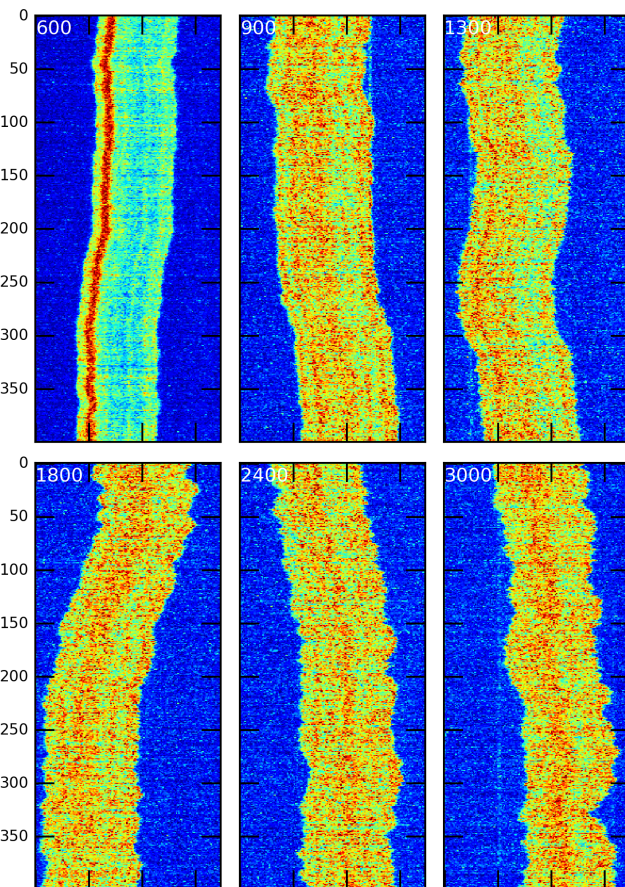


Figure 58: Vertical axis is time. White annotation gives channel width in nanometres.

3.30 130905-RecA-T4-wide-8

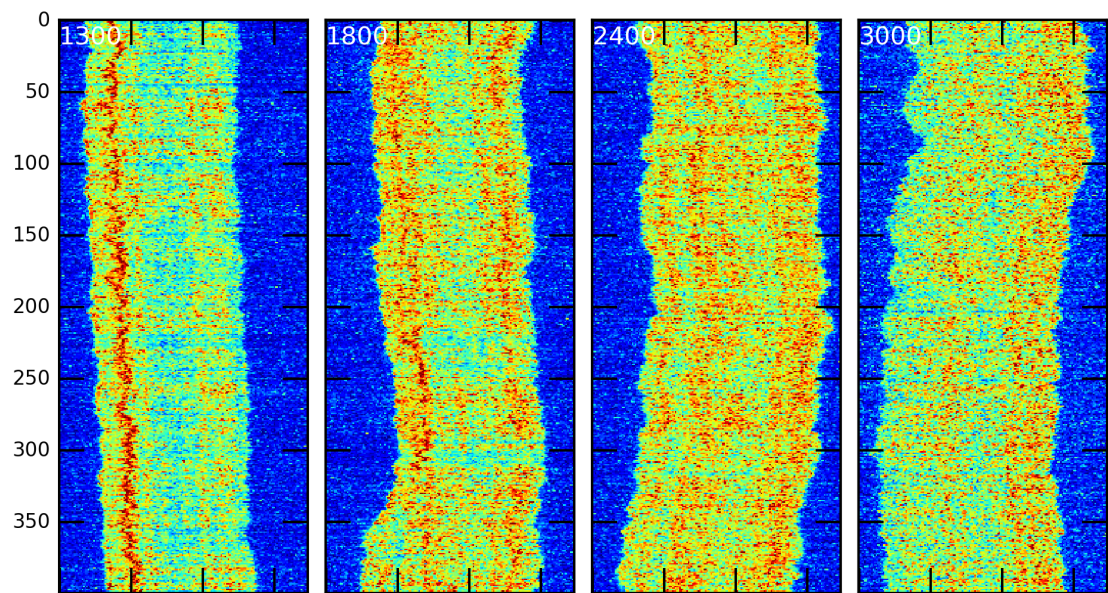


Figure 59: Vertical axis is time. White annotation gives channel width in nanometres.

3.31 130924-RecA-lambda-narrow-1

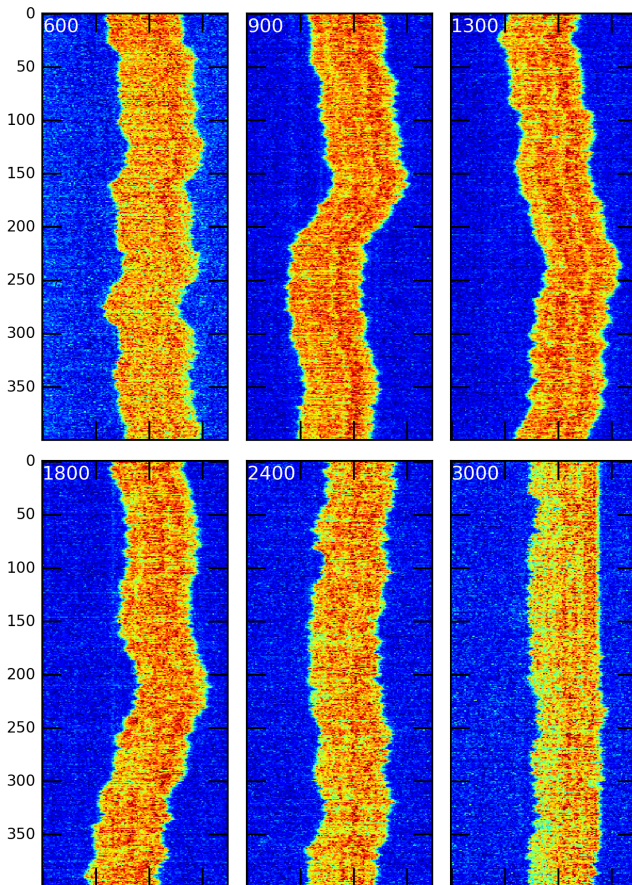


Figure 60: Vertical axis is time. White annotation gives channel width in nanometres.

3.32 130924-RecA-lambda-narrow-2

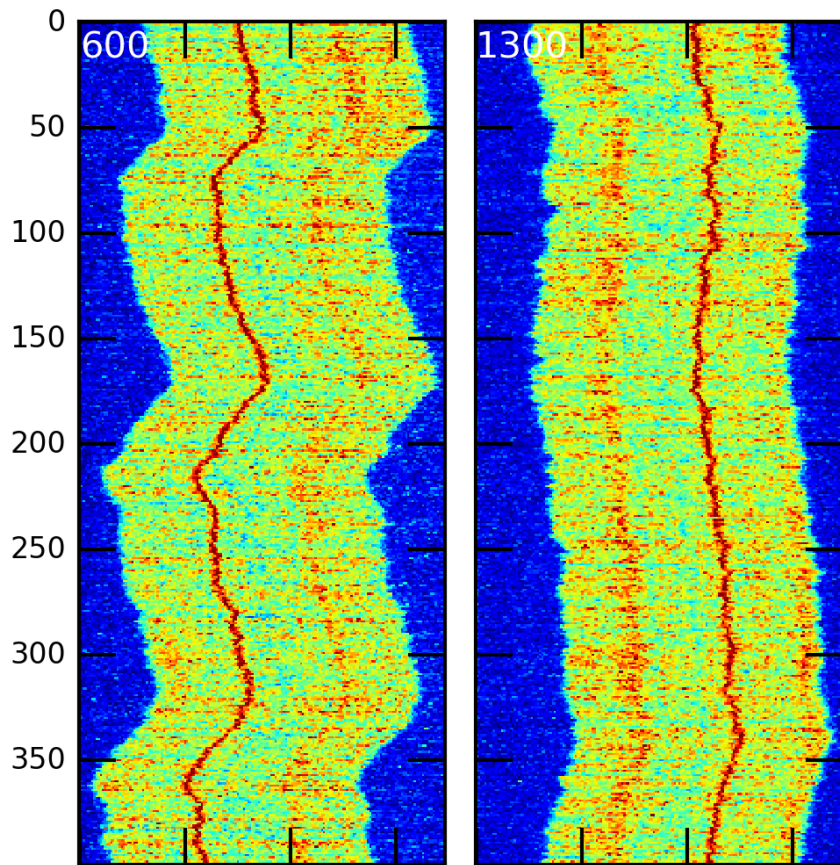


Figure 61: Vertical axis is time. White annotation gives channel width in nanometres.

3.33 130924-RecA-lambda-narrow-3

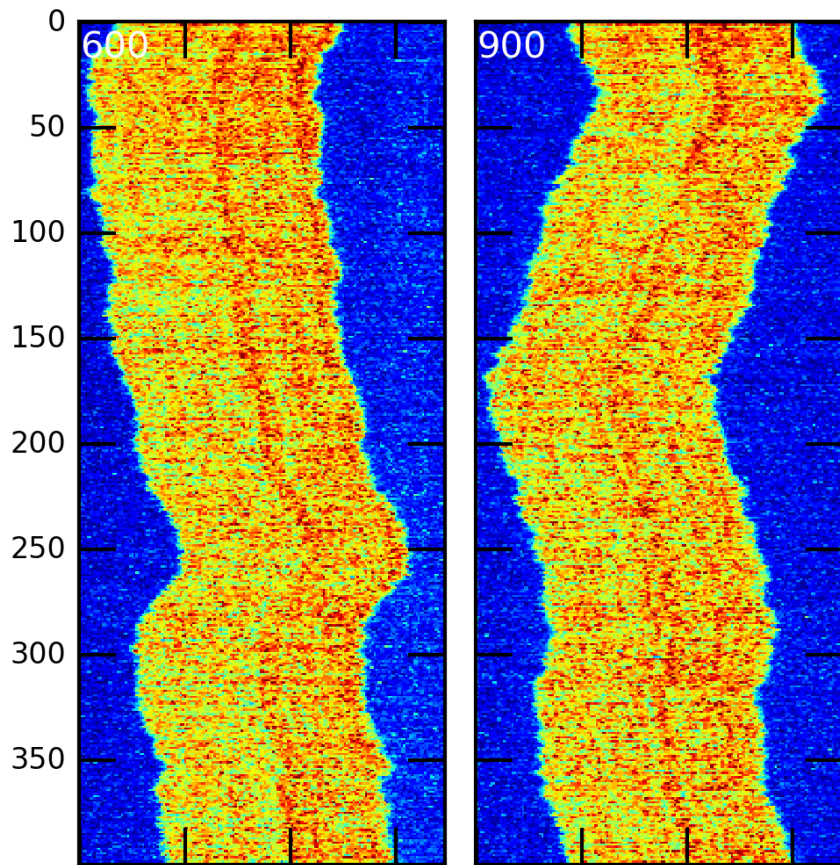


Figure 62: Vertical axis is time. White annotation gives channel width in nanometres.

3.34 130924-RecA-lambda-narrow-4

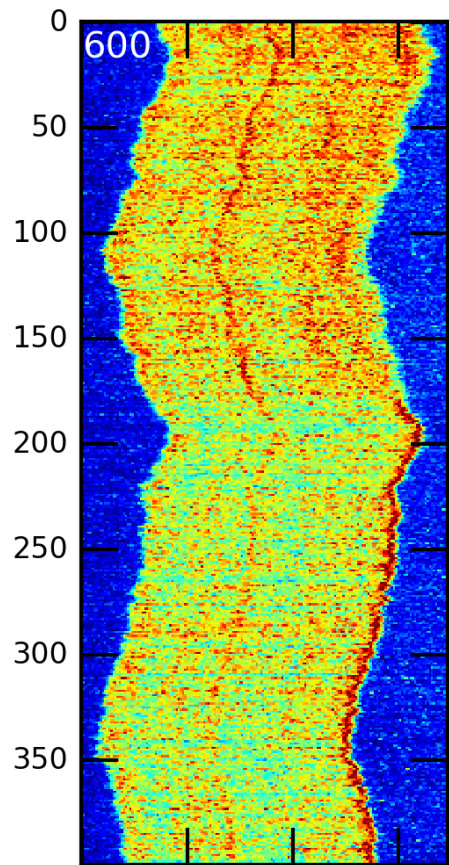


Figure 63: Vertical axis is time. White annotation gives channel width in nanometres.

3.35 130924-RecA-lambda-narrow-5

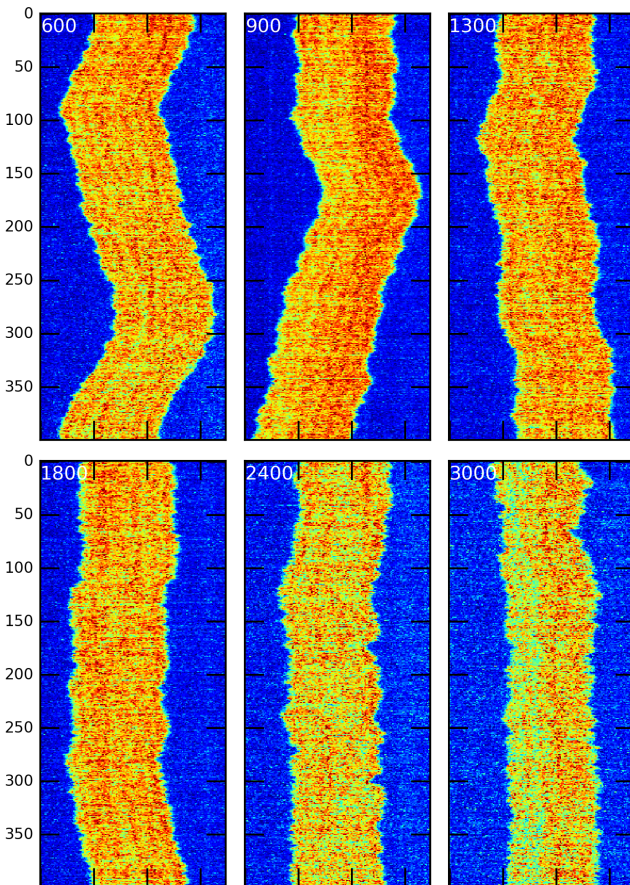


Figure 64: Vertical axis is time. White annotation gives channel width in nanometres.

3.36 130924-RecA-lambda-narrow-6

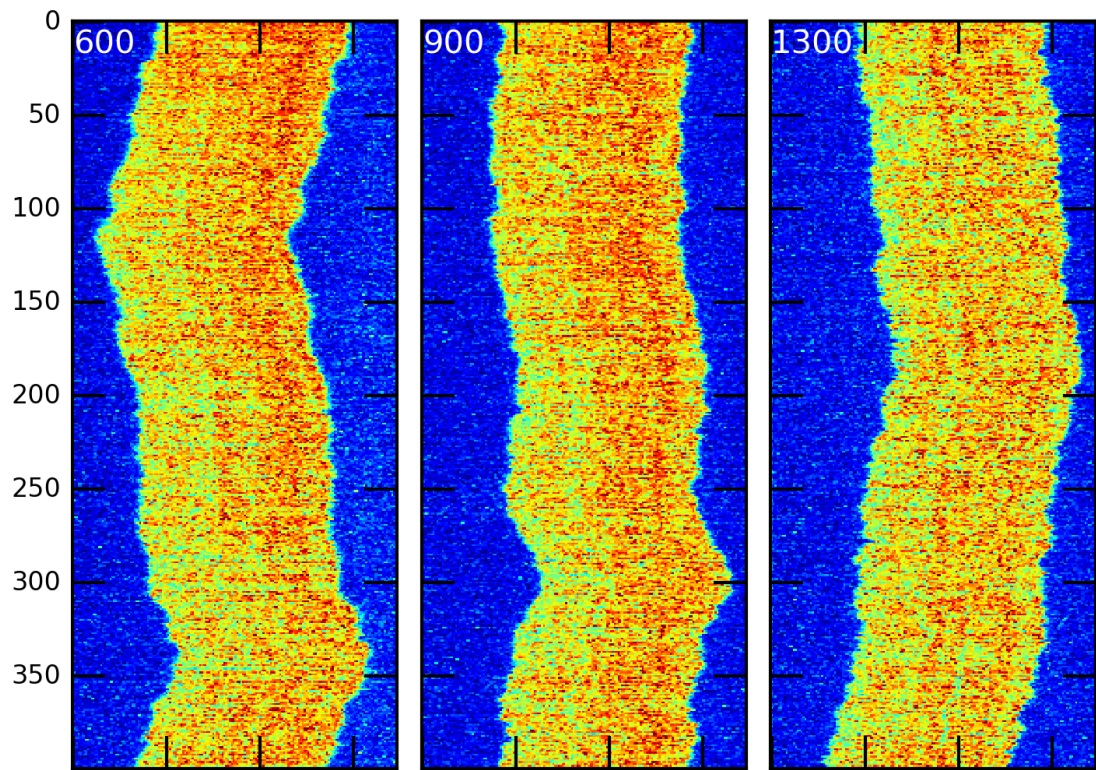


Figure 65: Vertical axis is time. White annotation gives channel width in nanometres.

3.37 130924-RecA-lambda-wide-1

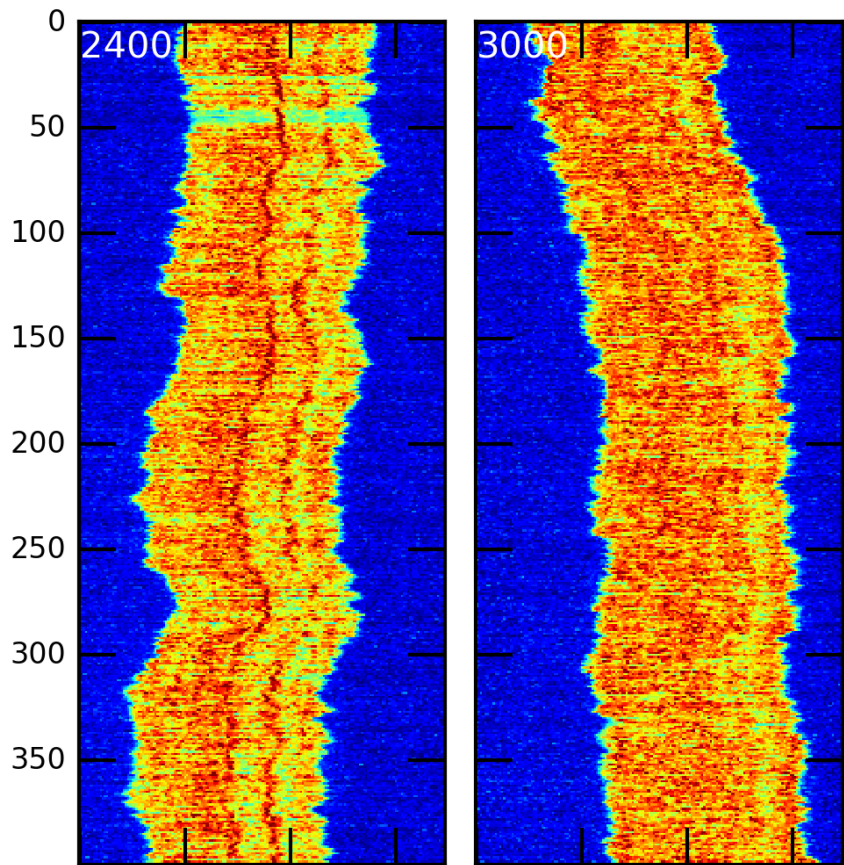


Figure 66: Vertical axis is time. White annotation gives channel width in nanometres.

3.38 130924-RecA-lambda-wide-10

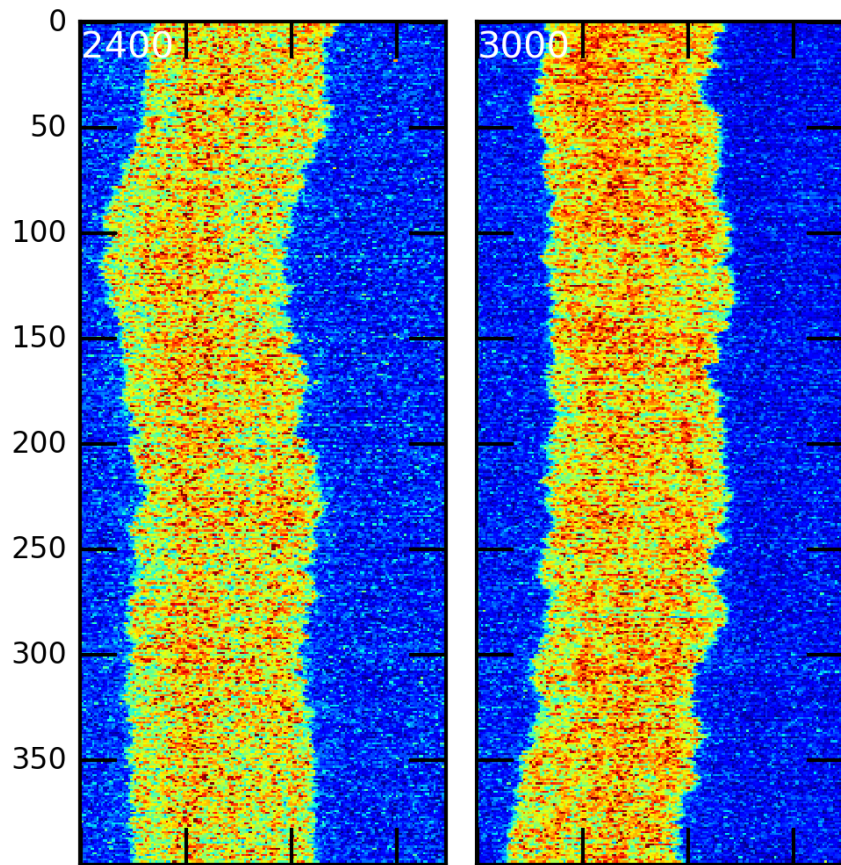


Figure 67: Vertical axis is time. White annotation gives channel width in nanometres.

3.39 130924-RecA-lambda-wide-2

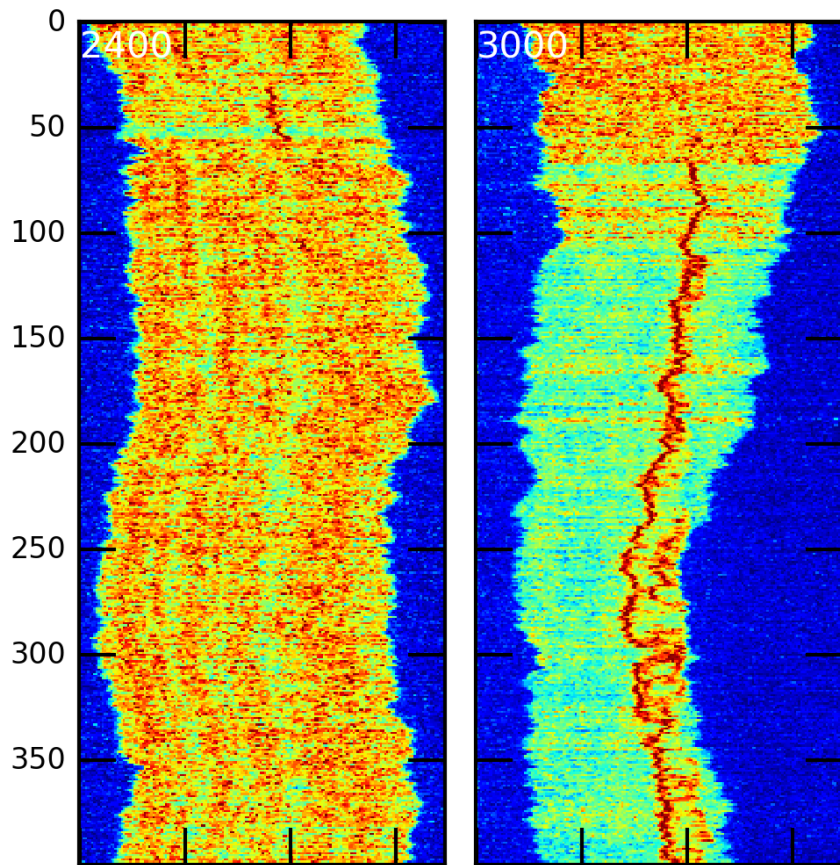


Figure 68: Vertical axis is time. White annotation gives channel width in nanometres.

3.40 130924-RecA-lambda-wide-3

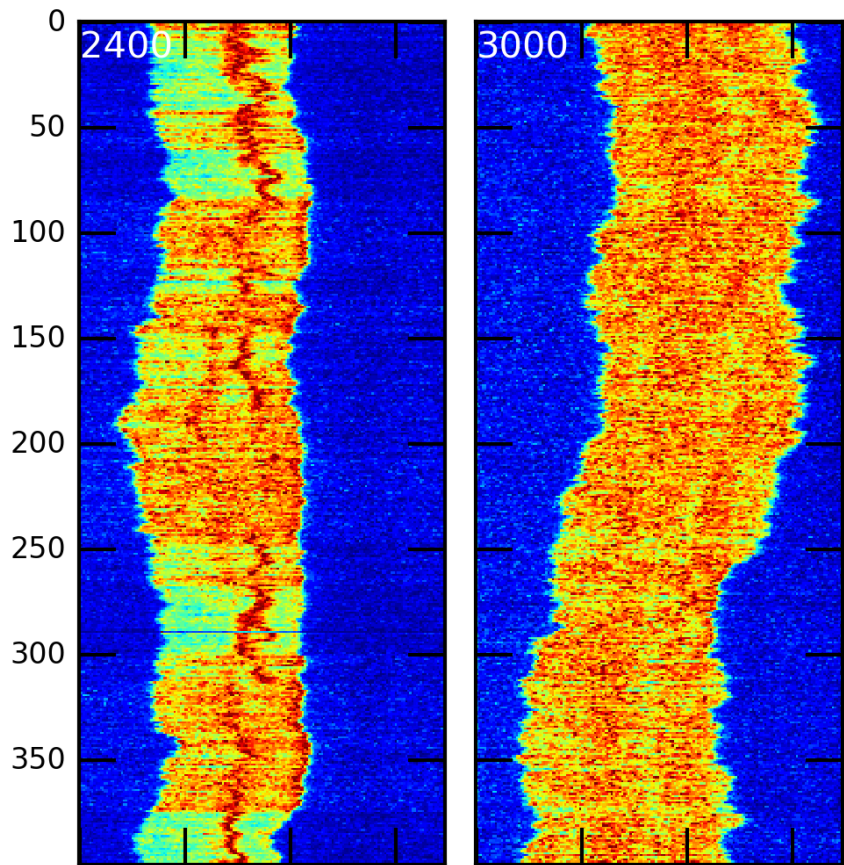


Figure 69: Vertical axis is time. White annotation gives channel width in nanometres.

3.41 130924-RecA-lambda-wide-4

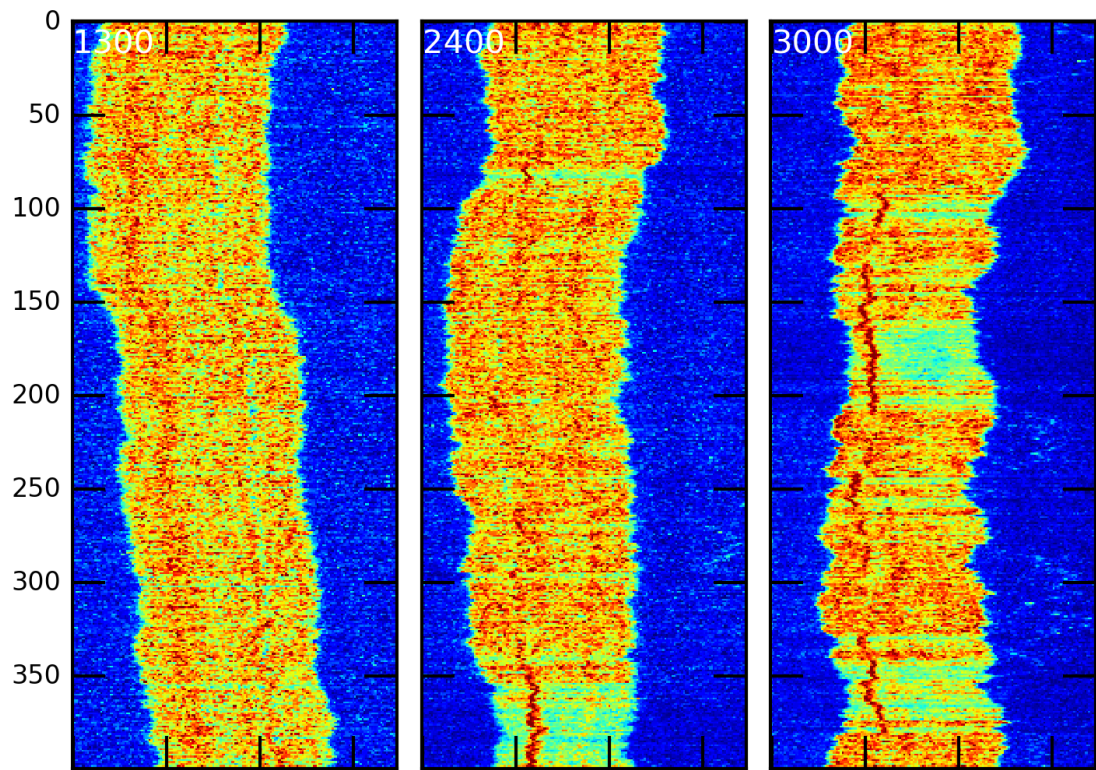


Figure 70: Vertical axis is time. White annotation gives channel width in nanometres.

3.42 130924-RecA-lambda-wide-5

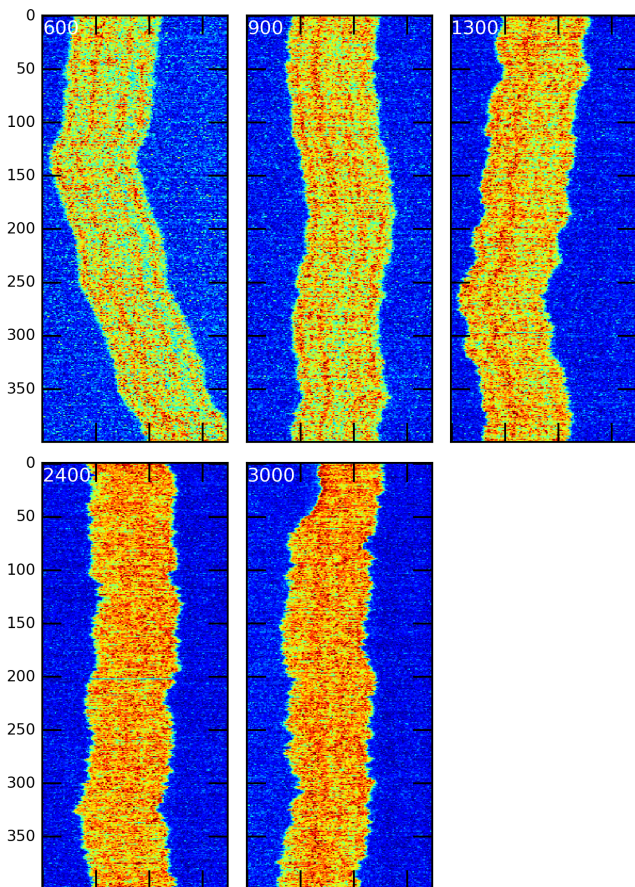


Figure 71: Vertical axis is time. White annotation gives channel width in nanometres.

3.43 130924-RecA-lambda-wide-8

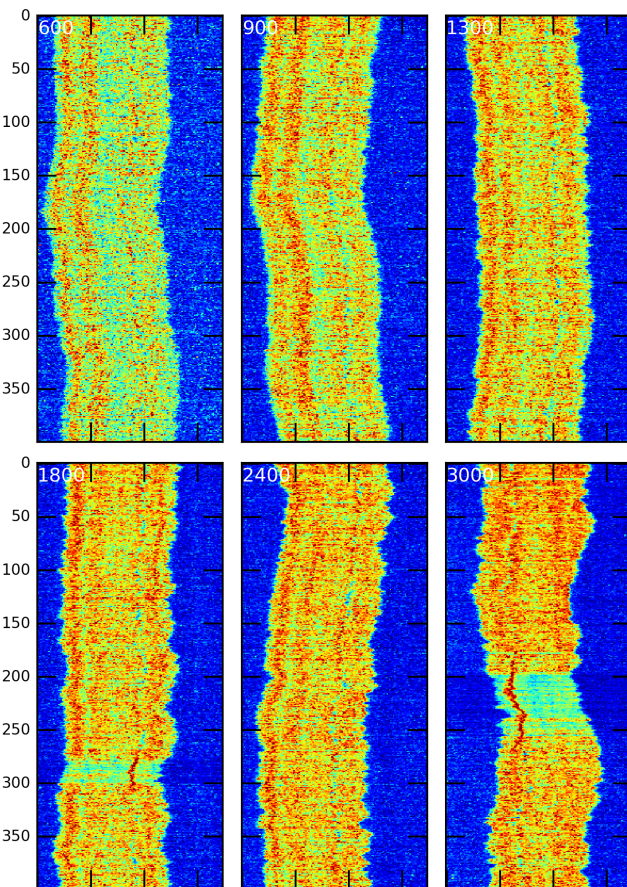


Figure 72: Vertical axis is time. White annotation gives channel width in nanometres.

3.44 130924-RecA-lambda-wide-9

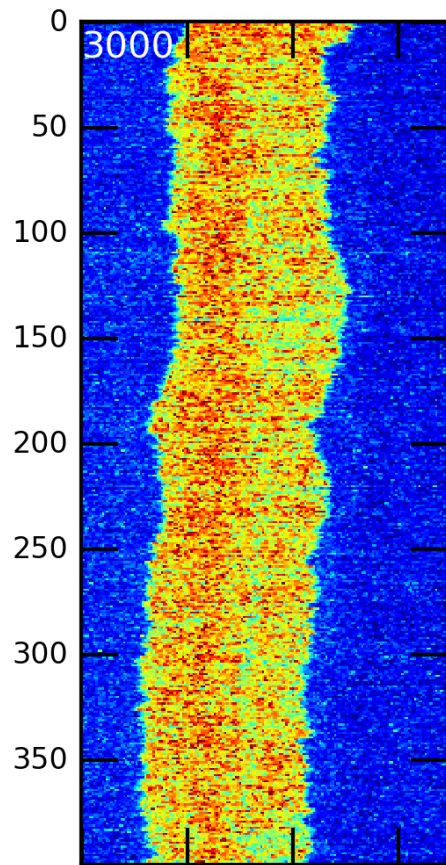


Figure 73: Vertical axis is time. White annotation gives channel width in nanometres.

References

- [1] K. Frykholm, M. Alizadehheidari, J. Fritzsche, J. Wigenius, M. Modesti, F. Persson, F. Westerlund, Probing physical properties of a dna-protein complex using nanofluidic channels, *Small* 10 (5) (2014) 884–887.
- [2] M. Hegner, S. B. Smith, C. Bustamante, Polymerization and mechanical properties of single reca-dna filaments, *Proceedings of the National Academy of Sciences* 96 (18) (1999) 10109–10114.